

A computational framework for fluid–structure interaction: Finite element formulation and applications

W. Dettmer, D. Perić *

Computational and Civil Engineering Research Centre, School of Engineering, University of Wales Swansea, Singleton Park, Swansea SA2 8PP, UK

Received 4 April 2005; received in revised form 17 October 2005; accepted 17 October 2005

Abstract

This work is concerned with the modelling of the interaction of fluid flow with flexible solid structures. The fluid flow considered is governed by the incompressible Navier–Stokes equations and modelled with stabilised low order velocity–pressure finite elements. The motion of the fluid domain is accounted for by an arbitrary Lagrangian–Eulerian (ALE) strategy. The structure is represented by means of an appropriate standard finite element formulation. For the temporal discretisation of both fluid and solid bodies, the discrete implicit generalised- α method is employed.

An important aspect of the presented work is the introduction of the independent interface discretisation, which allows an efficient, modular and expandable implementation of the solution strategy. A simple data transfer strategy based on a finite element type interpolation of the interface degrees of freedom guarantees kinematic consistency and equilibrium of the stresses along the interface.

The resulting strongly coupled set of non-linear equations is solved by means of a novel partitioned solution procedure, which is based on the Newton–Raphson methodology and incorporates the full linearisation of the overall incremental problem. Thus, asymptotically quadratic convergence of the residuals is achieved. Numerical examples are presented to demonstrate the robustness and efficiency of the methodology.

© 2006 Elsevier B.V. All rights reserved.

Keywords: Fluid–structure interaction; Arbitrary Lagrangian–Eulerian (ALE) formulation; Partitioned solution algorithm; Stabilised finite element method

1. Introduction

The interaction of fluid flow with flexible solid structures is frequently encountered in many areas of civil, mechanical, aerospace and biomechanical engineering. Traditional approaches to analysis of such problems, although proving extremely useful tools in engineering practice, necessarily rely on simplified models, which have narrow range of validity and applications [1]. More demanding fluid–structure interaction problems, such as those involving for instance large structural deformations, necessitate use of numerical approaches. In recent years the numerical modelling of fluid–structure interaction has become a focus of major research activity (see e.g. [2] for a recent review of the field). This has been made possible by the advances made during the last decade or so in enabling computational methodologies comprising both computational modelling of fluid flow and solid structures, and galvanised by further significant increases in terms of affordable computational resources. However, the optimal choice of specific numerical strategies for the discretisation of the fluid, solid and time domains and for the modelling of the fluid–structure interface still remains open. A number of different solution procedures for the coupled discretised problem are currently being employed [2].

* Corresponding author. Tel.: +44 1792 295542; fax: +44 1792 295676.
E-mail address: d.peric@swansea.ac.uk (D. Perić).

In this work, we propose a specific combination of numerical discretisation strategies and then present a novel solution procedure for the coupled sets of discrete non-linear equations. In particular, we employ a discrete time integration scheme as opposed to the recently frequently used space–time strategies. The adopted solution strategy allows the employment of independent interface degrees of freedom, which adds significantly to its efficiency, modularity and expandability. A major contribution of the present work is the development of a novel solution procedure based on the exact linearisation of the overall problem, which results in optimal rates of convergence of the residuals.

We point out that the work presented in this paper extends the solution methodologies described in [3,4] for fluid–rigid body interaction and free surface flows with surface tension to the problem of fluid–structure interaction. As a consequence of this, the presentation of the background material is largely common to all three publications. The close relation between the solution strategies we have employed in modelling of free surface flow [3] and fluid–rigid body interaction [4], and the strategy for fluid–structure interaction described in this paper, has been used in [5] for the development of a single computational platform with a wide range of applications.

The computational ingredients of the adopted strategy are as follows:

In this paper, we assume an incompressible Newtonian fluid. For the modelling of the fluid flow we therefore use a stabilised equal order velocity–pressure finite element formulation adapted to a moving domain. The stabilisation technique employed was introduced by Hughes and co-workers (see e.g. [6–8]) and then further developed by Tezduyar and others (see e.g. [9–12]). It enhances stability of the velocity field in advection dominated regions of the domain and at the same time enables the use of computationally convenient equal order finite element spaces for the velocity and pressure fields. The formulation used in this work is referred to as the *streamline-upwind*- and *pressure-stabilising*/Petrov–Galerkin method (SUPG/PSPG, see [9]), which, in the framework of linear finite element interpolation, may be regarded as a *Galerkin/least-squares* stabilisation technique (see [7]). Such techniques have become standard in Eulerian finite element formulations and have been applied to various problems arising in fluid mechanics (see e.g. [13,15–18,3,19,5]). A review of a variety of stabilisation techniques may be found in [20].

We emphasise that the solution strategy for fluid–structure interaction problems presented in this work is not limited to incompressible fluid flow applications. The stabilised formulation described above can be replaced by an appropriate finite element method for compressible fluid flow or, in fact, by a finite volume strategy. However, due to its relevance in physical applications, we have chosen to consider incompressible fluids. It has also been shown recently by Matthies [21] that the presence of the incompressibility constraint indeed makes this the more challenging problem.

An *arbitrary Lagrangian–Eulerian* (ALE) description is used to account for the deformation of the fluid domain which arises from the displacement and deformation of the solid structure. Some of the first researchers to demonstrate the potential of this approach are, among others, Hirt et al. [22], Hughes et al. [23], Donea [24], Ramaswamy and Kawahara [25,26], Huerta and Liu [27], Soulaimani et al. [28]. More recent publications are e.g. [29–32,18,3–5]. A related strategy based on the space–time finite element formulation on moving domains has been developed by Tezduyar et al. [33,34], Masud and Hughes [13] and Hansbo [14]. In all the above strategies the movement of the fluid finite element mesh is governed by an appropriate algorithm, thus maintaining a good mesh quality despite substantial deformation of the fluid domain.

The solid structure, depending on the physical problem under consideration, may be modelled by an appropriate standard finite element technique, involving membrane, beam, shell and/or continuum elements. The strategy adopted in this work allows the employment of non-matching fluid and structural meshes based on different finite element interpolations. At the interface a simple interpolation strategy is employed, which strongly enforces kinematic constraints and leads to a straightforward transfer of the traction fields. This methodology has been extended to incorporate the independent finite element type discretisation of the interface.

The *generalised- α* method is employed for the integration in time. This method belongs to the class of discrete and implicit single step integration schemes. For linear problems the scheme can be shown to be second order accurate and unconditionally stable. Furthermore, it allows strict user controlled damping of high unresolved frequencies. The generalised- α method was originally developed for the second order problems arising in solid dynamics by Chung and Hulbert [35], and later adapted to the first order problems typically encountered in Eulerian fluid dynamics by Jansen et al. [36]. For a detailed study of the generalised- α method in the context of the stabilised Eulerian finite element formulation for fluid flow we refer to [37,5]. In this work, we employ the original generalised- α scheme introduced in [35] for the time integration of the structural dynamics, whereas we base the integration of the fluid flow on [36,37].

The fully discretised model consists of coupled sets of non-linear equations. The coupling can be described briefly as follows: The deformation of the structure is driven by the traction forces exerted by the fluid at the fluid–solid interface. The structural displacements, on the other hand, define the geometry and the geometry changes of the fluid domain. In a discrete finite element setting this situation may be regarded as a coupled three field problem, involving the fluid flow, the motion of the fluid mesh and the structural dynamics.

The final numerical ingredient required is a robust and efficient solution procedure to compute the complete set of unknowns at the current time instant. Due to the above described coupling, this poses a considerable difficulty, which

is often circumvented by the employment of staggered partitioned solution schemes (for more information on this approach see [38]). Such techniques require the execution of a specified sequence of solver components with intermediate communication of data. However, these methods often lack accuracy and robustness, and thereby impose a restriction to small time steps. Alternatively, a specified sequence of solver components may be iteratively repeated until accuracy requirements are met [39,40]. In the experience of the authors, the iterative schemes from this category usually exhibit poor convergence, particularly for large fluid meshes and soft structures. In this work, a *novel partitioned solution scheme* has been developed relying on the Newton–Raphson procedure, which incorporates the full linearisation of the incremental problem and hence exhibits asymptotically quadratic convergence of the solution for all problem unknowns. Alternative strategies, some of which resemble Quasi-Newton procedures or employ linearisations obtained by numerical differentiation, have been suggested by e.g. Tezduyar [41,42] and Matthies and Steindorf [40].

It will be shown in the following sections that the combination of the above described numerical ingredients renders a robust, accurate and competitive methodology. A specific focus of this work is on the solution procedure employed to resolve the strong coupling of the problems under consideration.

The layout of the paper is as follows: In Section 2 we summarise the governing equations. The fluid finite element formulation is presented in Section 3. Subsequently, we discuss the update strategy for the fluid mesh. In Section 5, some remarks are made on the structural finite element methods considered in this work. Section 6 is concerned with the integration in time, and in Section 7 we address the modelling of the interface and establish a compact representation of the overall discretised coupled and non-linear problem. The solution strategy is then discussed in Section 8. Finally, three numerical examples are presented in detail in Section 9.

2. Governing equations

2.1. Incompressible Newtonian fluid flow on a moving domain

2.1.1. The moving reference frame

An essential feature of the problems under consideration is the motion of the boundary of the fluid domain. The geometry of the fluid domain may change substantially during the time domain of interest. The fluid particles flow in or through a spatial domain, which is itself at motion. Therefore, it is convenient to formulate the problem in the ALE description relying on a moving reference frame, in which the conservation laws are expressed.

In this context it is well-established (see e.g. [3,4,19,22–25]) that the time derivative of the velocity \mathbf{u} of the fluid particle which traverses through the coordinate $\hat{\mathbf{x}}$ of the reference frame at a specific time instant can be written as

$$\frac{D\mathbf{u}}{Dt} = \nabla_{\hat{\mathbf{x}}}\mathbf{u}(\mathbf{u} - \hat{\mathbf{v}}) + \dot{\mathbf{u}}, \quad (1)$$

where $\hat{\mathbf{v}} = \partial\hat{\mathbf{x}}/\partial t$ is the velocity of the reference point.

The operator $\nabla_{\hat{\mathbf{x}}}(\bullet)$ denotes the derivatives with respect to the current referential coordinates $\hat{\mathbf{x}}$. The expression $\dot{\mathbf{u}}$ corresponds to the change of the material particle velocity, which is noted by an observer travelling with a point on the reference frame. The velocity difference $\mathbf{u} - \hat{\mathbf{v}}$ is denoted as the *convective velocity*. In the framework of the finite element method, the moving reference frame is identified with the finite element mesh. The Eulerian or Lagrangian representations of the material time derivative of \mathbf{u} are easily recovered from (1) by setting $\hat{\mathbf{v}} = \mathbf{0}$ or $\hat{\mathbf{v}} = \mathbf{u}$, respectively.

2.1.2. Governing equations

The momentum conservation law and the continuity equation for incompressible flow are formulated in the referential description as

$$\rho(\dot{\mathbf{u}} + (\nabla_{\hat{\mathbf{x}}}\mathbf{u})(\mathbf{u} - \hat{\mathbf{v}}) - \mathbf{f}) - \nabla_{\hat{\mathbf{x}}} \cdot \boldsymbol{\sigma} = \mathbf{0} \quad \forall(\hat{\mathbf{x}}, t) \in \Omega \times I, \quad (2)$$

$$\nabla_{\hat{\mathbf{x}}} \cdot \mathbf{u} = 0 \quad \forall(\hat{\mathbf{x}}, t) \in \Omega \times I, \quad (3)$$

where ρ , \mathbf{f} and $\boldsymbol{\sigma}$ represent, respectively, the fluid density, the volume force vector and the Cauchy stress tensor. The time interval of interest is denoted as $I = [0, T]$. The constitutive equation for the Newtonian fluid, to which this work is restricted, reads

$$\boldsymbol{\sigma} = -p\mathbf{I} + 2\mu\nabla_{\hat{\mathbf{x}}}^s\mathbf{u}, \quad (4)$$

where \mathbf{I} is the second order identity tensor, μ denotes the fluid viscosity, $\nabla_{\hat{\mathbf{x}}}^s(\bullet)$ is the symmetric gradient operator and p represents the pressure, which, in similarity to the velocity \mathbf{u} , is a function of $\hat{\mathbf{x}}$ and t .

The boundary Γ of Ω may consist of the complementary subsets Γ_g , Γ_h and Γ_{f-s} , which represent the following boundary conditions

$$\mathbf{u} - \mathbf{g} = \mathbf{0} \quad \forall(\hat{\mathbf{x}}, t) \in \Gamma_g \times I, \tag{5}$$

$$\boldsymbol{\sigma}\hat{\mathbf{n}} - \mathbf{h} = \mathbf{0} \quad \forall(\hat{\mathbf{x}}, t) \in \Gamma_h \times I, \tag{6}$$

$$\mathbf{u} - \dot{\mathbf{d}} = \mathbf{0} \quad \forall(\hat{\mathbf{x}}, t) \in \Gamma_{f-s} \times I, \tag{7}$$

$$(\mathbf{u} - \hat{\mathbf{v}}) \cdot \hat{\mathbf{n}} = 0 \quad \forall(\hat{\mathbf{x}}, t) \in \Gamma_{f-s} \times I, \tag{8}$$

$$\mathbf{t}_f + \mathbf{t}_s = \boldsymbol{\sigma}\hat{\mathbf{n}} + \mathbf{t}_s = \mathbf{0} \quad \forall(\hat{\mathbf{x}}, t) \in \Gamma_{f-s} \times I. \tag{9}$$

The quantities \mathbf{g} , \mathbf{h} and $\hat{\mathbf{n}}$ denote, respectively, prescribed velocity and traction vectors and the current outward normal unit vector of the boundary, which is given by the positions $\hat{\mathbf{x}}$ of the boundary. For most practical applications the Dirichlet and Neumann boundaries Γ_g and Γ_h are fixed in space and thus $\hat{\mathbf{v}} = \mathbf{0}$ or at least $\hat{\mathbf{v}} \cdot \hat{\mathbf{n}} = 0$ on Γ_g and Γ_h , $\forall t \in I$.

Eq. (7) represents the no-slip condition at the fluid–structure interface Γ_{f-s} . The quantity $\dot{\mathbf{d}}$ denotes the velocity vector field of the structure at the interface Γ_{f-s} . Also on Γ_{f-s} , the velocity $\hat{\mathbf{v}}$ of the reference frame and the positions $\hat{\mathbf{x}}$ need to satisfy the consistency condition (8), which ensures that the boundary of the reference frame accurately represents the current configuration of the structure. The equilibrium of the stresses along the interface is expressed by the relation (9), where the quantities \mathbf{t}_f and \mathbf{t}_s represent the traction vectors exerted, respectively, by the fluid and the structure on the interface.

Finally, we note the initial conditions $\mathbf{u} = \mathbf{u}_0$, $\dot{\mathbf{u}} = \dot{\mathbf{u}}_0$ and $\hat{\mathbf{x}} = \hat{\mathbf{x}}_0$, $\forall \hat{\mathbf{x}} \in \Omega$ at $t = 0$.

2.2. Structural dynamics

In a standard Lagrangian description, the conservation of momentum of a solid continuum may be expressed in spatial description as

$$\rho(\ddot{\mathbf{d}} - \mathbf{f}) - \nabla \cdot \boldsymbol{\sigma} = \mathbf{0}, \tag{10}$$

where ρ is the current density of the deformed solid and the vector \mathbf{d} represents the displacement field, whereas the body forces are given by the vector \mathbf{f} . The symmetric second order tensor $\boldsymbol{\sigma}$ in (10) denotes the Cauchy stress tensor. Following standard finite strain continuum mechanics, appropriate local strain measures may be defined on the basis of the displacement field \mathbf{d} . The Cauchy stress $\boldsymbol{\sigma}$ is related to the strains by a constitutive relation suitable to model the behaviour of the solid material under consideration. For simplicity, this work shall be restricted to elastic structures (see Section 5).

In similarity to the boundary of the fluid domain, the boundary of the solid structure may consist of three complementary subsections Γ_h , Γ_d and Γ_{f-s} with

$$\mathbf{d} - \mathbf{g} = \mathbf{0} \quad \forall(\mathbf{x}, t) \in \Gamma_g \times I, \tag{11}$$

$$\boldsymbol{\sigma}\mathbf{n} - \mathbf{h} = \mathbf{0} \quad \forall(\mathbf{x}, t) \in \Gamma_h \times I, \tag{12}$$

$$\dot{\mathbf{d}} - \mathbf{u} = \mathbf{0} \quad \forall(\mathbf{x}, t) \in \Gamma_{f-s} \times I, \tag{13}$$

$$\mathbf{t}_s + \mathbf{t}_f = \boldsymbol{\sigma}\mathbf{n} + \mathbf{t}_f = \mathbf{0} \quad \forall(\mathbf{x}, t) \in \Gamma_{f-s} \times I, \tag{14}$$

where the quantities \mathbf{g} , \mathbf{h} and \mathbf{n} denote, respectively, prescribed displacement and traction vectors and the current outward normal unit vector of the boundary. The boundary conditions (13) and (14) clearly correspond to (7) and (9), respectively.

Initially, the configuration of the structure is known as $\mathbf{d} = \mathbf{d}_0$ and $\dot{\mathbf{d}} = \dot{\mathbf{d}}_0$ $\forall \mathbf{x} \in \Omega$ at $t = 0$.

3. Stabilised finite element formulation for the fluid flow

Let \mathcal{S}^h , \mathcal{V}^h , \mathcal{P}^h be the appropriate finite element spaces of continuous piecewise linear functions on Ω^h , where $\Omega^h = \bigcup_{e=1}^{n_{el}} \Omega^e$ is a standard discretisation of the fluid domain Ω with n_{el} finite elements. A stabilised velocity–pressure finite element formulation of the fluid flow described in Section 2.1 then reads:

For any $t \in I$, find $\mathbf{u}^h \in \mathcal{S}^h$ and $p^h \in \mathcal{P}^h$ such that the following weak form is satisfied for any admissible $\delta \mathbf{u}^h \in \mathcal{V}^h$ and $\delta p^h \in \mathcal{P}^h$,

$$G^f(\mathbf{u}^h, p^h; \delta \mathbf{u}^h, \delta p^h) = G_{Gal}(\mathbf{u}^h, p^h; \delta \mathbf{u}^h, \delta p^h) + G_{stab}(\mathbf{u}^h, p^h; \delta \mathbf{u}^h, \delta p^h) = 0. \tag{15}$$

The variational form (15) consists of the standard Galerkin terms summarised in G_{Gal} , to which a stabilisation term G_{stab} of the momentum equation has been added.

In order to simplify the notation in the remainder of this section, which is dedicated to the detailed presentation of G_{Gal} and G_{stab} , the coupling of Eq. (15) with the deformation of the solid structure is not explicitly included. This issue, together with the appropriate notation, is elaborated in detail in Section 7.

The Galerkin terms, which can be obtained from Eqs. (2)–(6) by the standard procedure, read

$$G_{\text{Gal}}(\mathbf{u}^h, p^h; \delta \mathbf{u}^h, \delta p^h) = \int_{\Omega^h} (\rho \delta \mathbf{u}^h \cdot (\dot{\mathbf{u}}^h + (\nabla_{\hat{\mathbf{x}}^h} \mathbf{u}^h)(\mathbf{u}^h - \hat{\mathbf{v}}^h) - \mathbf{f}) + \nabla_{\hat{\mathbf{x}}^h} \delta \mathbf{u}^h : \boldsymbol{\sigma}(\mathbf{u}^h, p^h) + \delta p^h (\nabla_{\hat{\mathbf{x}}^h} \cdot \mathbf{u}^h)) \, dv - \int_{\Gamma_h^h} \delta \mathbf{u}^h \cdot \mathbf{h}^h \, da, \quad (16)$$

where the vector field $\hat{\mathbf{v}}^h$ denotes the mesh motion, which is based on the same finite element interpolation as \mathbf{u}^h .

The stabilisation term used in this work is similar to the one employed by the authors in [9], but has been extended to incorporate modifications required in the ALE framework. In [9], the stabilisation technique is referred to as a combination of the *streamline-upwind*- and the *pressure-stabilising/Petrov–Galerkin* schemes (SUPG/PSPG).

The stabilisation serves two purposes: First, it provides stability to the velocity field \mathbf{u}^h in convection dominated regions of the domain. Second, it circumvents the Babuška–Brezzi condition, which standard mixed Galerkin methods are required to satisfy. Thus, it effectively renders a smooth pressure field without jeopardising the weak enforcement of the continuity condition.

The stabilisation term employed here reads

$$G_{\text{stab}}(\mathbf{u}^h, p^h; \delta \mathbf{u}^h, \delta p^h) = \sum_{e=1}^{n_{\text{el}}} \int_{\Omega^e} [\tau_u \rho (\nabla_{\hat{\mathbf{x}}^e} \delta \mathbf{u}^h)(\mathbf{u}^h - \hat{\mathbf{v}}^h) + \tau_p \nabla_{\hat{\mathbf{x}}^e} \delta p^h] \cdot [\rho (\dot{\mathbf{u}}^h + (\nabla_{\hat{\mathbf{x}}^e} \mathbf{u}^h)(\mathbf{u}^h - \hat{\mathbf{v}}^h) - \mathbf{f}) + \nabla_{\hat{\mathbf{x}}^e} p^h] \, dv. \quad (17)$$

We note that due to the absence of the viscous term in the second pair of brackets in (17), the stabilisation term does not vanish as the spatial discretisation is refined. Consequently, the choice of the weighting parameter τ and its limit behaviour are essential for the success of the methodology. In the experience of the authors, it has proved useful (see also e.g. [9]) to employ two parameters, here denoted as τ_u and τ_p , and hence treat the two stabilisation purposes separately.

Both stabilisation parameters τ_u and τ_p are defined as follows:

$$\tau = \frac{h^e}{2 \|\mathbf{u}^e - \hat{\mathbf{v}}^e\| \rho} z, \quad z = \frac{\beta_1}{\sqrt{1 + \left(\frac{\beta_1}{\beta_2 Re^e}\right)^2}}, \quad Re^e = \frac{\|\mathbf{u}^e - \hat{\mathbf{v}}^e\| h^e \rho}{2\mu}, \quad (18)$$

but they have different scaling parameters β_1 and β_2 , which may be set independently. The characteristic element size, the convective velocity in the element centroid and the element Reynolds number are represented by h , $\mathbf{u}^e - \hat{\mathbf{v}}^e$, and Re^e , respectively. Thus, τ_u and τ_p are constant within every element and, hence, the stabilisation terms are discontinuous across the inter element boundaries, which explains the summation of integrals in (17). The parameters β_1 and β_2 define the limit of z as $Re^e \rightarrow \infty$ and the derivative dz/dRe^e at $Re^e = 0$, respectively. The examples in Section 9 have all been obtained with $(\beta_1 = 1, \beta_2 = \frac{1}{3})$ for τ_u and $(\beta_1 = 30, \beta_2 = \frac{1}{10})$ for τ_p . This specific choice makes the parameter τ_u identical to the expression which yields nearly exact solutions for the one-dimensional advection–diffusion equation (see [6] and references therein). In this work, the characteristic element size h^e is defined as the diameter of the circle, the area of which corresponds to the finite element e .

The choice of the formula in (18) is rather heuristic, and many different expressions have been introduced in literature (see e.g. [9,12,37,43]). In some early publications (e.g. [9]) it was suggested that τ should vanish as the discretisation in time is refined. In the context of a finite difference time integration scheme, the expressions (18), which do not depend on the time increment, have been shown to yield a robust method, allowing, to a wide extent, independent refinement of the discretisations of space and time (see [37] for a more detailed discussion and numerical verification).

4. Motion of the fluid finite element mesh

At this stage, the motion of the fluid mesh is arbitrary except for its outline: On the interface boundary Γ_{f-s}^h , Eq. (8) has to be satisfied. On the other parts of Γ^h , the user prescribes at least the motion of the nodes normal to the current configuration of the boundary. Note that, eventually, there may be regions of Ω^h , which are not required to adapt to a new geometry, since they are far away from the moving structure. In such regions we set $\hat{\mathbf{v}}^h = \mathbf{0}$, and the flow problem becomes purely Eulerian.

4.1. Motion of internal nodes

The movement of the internal finite element nodes should be chosen such that the mesh quality does not deteriorate as the displacements of the solid structure become large. For this purpose, many different algorithms have been suggested in literature (see e.g. [44–46,5] and references therein).

In this work the following techniques are used:

- *Pseudo-elastic technique.* In this approach, the mesh is simply assumed to represent an elastic solid body. A standard Lagrangian finite element technique typically employed in solid mechanics can then be used to adapt the mesh to the new geometry of the domain. For small distortions of the geometry the linear elastic model is sufficient. In the presence of large deformations of the fluid domain a hyperelastic model may be more suitable. Note that the mesh need not necessarily represent an elastic continuum. In literature, alternative methodologies have been suggested in which the mesh is, for example, assumed to be a network of elastic springs (see e.g. [46] and references therein). In the pseudo-elastic approach used in this work, the mesh is treated as a simple hyperelastic Neo–Hookean continuum, with two parameters μ^m and K^m , representing the shear and bulk modulus, respectively. For the two-dimensional situation the plane strain condition is employed.
- *Optimisation of mesh quality.* A simple strategy to compute the mesh motion can be defined by enforcing the condition, which requires that the mesh quality, with respect to a certain criteria, is optimal at all times $t \in I$. In this work, the chosen criteria is the ratio of the inner and outer circles of the triangular or tetrahedral finite element. Thus, the mesh movement satisfies

$$W = \sum_{e=1}^{n_{el}} \left(\frac{r_{out}^e}{r_{in}^e} \right) \Rightarrow \text{MIN}, \tag{19}$$

which is a simplified version of the expression used in [31]. The quantities r_{in}^e and r_{out}^e denote the inner and the outer radii of a triangular or tetrahedral finite element. The equations, which determine the nodal positions $\hat{\mathbf{x}}_i^f$, then read

$$\frac{\partial W}{\partial \hat{\mathbf{x}}_i^f} = \mathbf{0}, \quad i = 1, 2, \dots, N^f, \tag{20}$$

where N^f denotes the number of nodes in the mesh interior. In the authors’ experience this methodology renders acceptable meshes even for very distorted geometries. Note that also the initial mesh should satisfy (19).

Both strategies can be fully linearised and thus allow the employment of the Newton–Raphson procedure to solve for the new nodal positions. This is of particular importance with respect to the overall solution procedure described in Section 8.

The employment of large time steps in problems involving severe deformations of the domain often requires the adaptation of the mesh to substantial changes of the geometry within one time step. In such cases the Newton–Raphson procedure may fail to converge. In this work, this problem is overcome by increment cutting within the mesh update procedure, i.e. the new displacement of the boundary is applied in increments if necessary.

4.2. Motion of nodes on the interface boundary

Provided that the initial boundary of the fluid mesh resolves “nicely” the surface of the solid structure, there is normally no need to allow for any tangential movement of the fluid nodes along the interface. The fluid mesh boundary, similarly to the fluid particles, can then be required to “stick” to the surface of the structure. Thus, we satisfy Eqs. (7) and (8) by employing a purely Lagrangian description of the interface, i.e.

$$\hat{\mathbf{v}}^h = \mathbf{u}^h = \mathcal{I}(\dot{\mathbf{d}}^h) \quad \forall (\hat{\mathbf{x}}^h, t) \in \Gamma_{f-s}^h \times I, \tag{21}$$

where the vector $\dot{\mathbf{d}}^h$ denotes the finite element approximation of the structural velocity field $\dot{\mathbf{d}}$. In order to allow for non-matching fluid and structural meshes, it is necessary to define an appropriate interpolation operator $\mathcal{I}(\bullet)$. This issue is addressed in detail in Section 7.

The current configuration of the interface boundary Γ_{f-s}^h is then described by

$$\hat{\mathbf{x}}^h = \mathcal{I}(\mathbf{x}_{s0}^h + \mathbf{d}^h) \quad \forall (\hat{\mathbf{x}}^h, t) \in \Gamma_{f-s}^h \times I, \tag{22}$$

where \mathbf{x}_{s0}^h denotes the discretisation of the initial configuration of the solid structure.

5. Finite element formulation for the solid structure

The fluid–structure interaction solution methodology adopted in this work does not impose any restriction on the specific choice of structural element to be used. Importantly, the structural mesh at the interface is not required to match the fluid finite element mesh. Thus, any appropriate standard finite element method may be used for the discretisation of the solid structure.

The starting point of a structural finite element method is the balance of momentum as given by (10) or by an appropriate equivalent representation. A standard finite element formulation of (10) reads as follows: For any $t \in I$, find $\mathbf{d}^h \in \mathcal{S}^h$ such that for any $\delta \mathbf{d} \in \mathcal{V}^h$

$$G^S(\mathbf{d}^h; \delta \mathbf{d}^h) = \int_{\Omega^h} (\delta \mathbf{d}^h \rho (\dot{\mathbf{d}}^h - \mathbf{f}) + \nabla \delta \mathbf{d}^h : \boldsymbol{\sigma}(\mathbf{d}^h)) dv - \int_{\Gamma_h^h} \delta \mathbf{d}^h \cdot \mathbf{h}^h da = 0, \quad (23)$$

where \mathcal{S}^h and \mathcal{V}^h are the appropriate finite element spaces and Ω^h is a finite element discretisation of the solid domain.

Introducing the vector of the nodal displacements \mathbf{d} , the formulation (23) can be rewritten in an equivalent matrix form as

$$\mathbf{M}\ddot{\mathbf{d}} + \mathbf{C}\dot{\mathbf{d}} + \mathbf{K}\mathbf{d} = \mathbf{P}, \quad (24)$$

where the matrices \mathbf{M} , \mathbf{C} and \mathbf{K} are denoted, respectively, as the mass, damping and stiffness matrices. It should be noted that some structural finite elements, such as beam and shell elements, also include the rotational degrees of freedom in addition to the translational displacements. We assume such rotations to be included in the vector \mathbf{d} .

6. Integration in time

In order to complete the discretisation of the finite element formulations (15) and (23), it remains to apply a numerical time integration scheme. The most popular choices are standard *discrete* time stepping schemes and the so-called *time finite element methods*. In the context of fluid mechanics, both approaches have been extensively discussed in recent publications (see e.g. [26,31] for discrete and [7,13,50] for time finite element methods).

In [37,5], we have provided a detailed comparison of implicit time integration schemes with respect to incompressible Newtonian fluid flow in the Eulerian framework. As a result, the discrete *generalised- α* method has been suggested as a very efficient and robust alternative to the more expensive time finite element methods. The generalised- α method has originally been developed in [35] for the second order differential equation arising in solid dynamics, but has been adapted to the first order problem of fluid mechanics in [36]. For linear problems the scheme can be shown to be unconditionally stable and second order accurate (see [35–37]). Furthermore, it enables user-controlled high frequency damping, which is desirable especially for coarse discretisation in space and time. This is achieved by specifying the single integration parameter, which, for linear problems, can be identified with the spectral radius ρ_∞ associated with very large time steps. In the following the application of the generalised- α method to Eqs. (15) and (23) is described.

First, the time interval $I = [0, T]$ is replaced by a sequence of discrete time instants t_n , $n = 0, 1, 2, \dots, N_{\text{time}}$ with $t_0 = 0$ and $t_{N_{\text{time}}} = T$. The time step size $\Delta t = t_{n+1} - t_n$ is allowed to vary.

6.1. Fluid solver

The generalised- α method is used to express \mathbf{u}^h and its time derivative $\dot{\mathbf{u}}^h$ in (15) in terms of \mathbf{u}^h and $\dot{\mathbf{u}}^h$ at the discrete time instants t_n and t_{n+1} . These values are henceforth denoted as $\mathbf{u}_n^h, \mathbf{u}_{n+1}^h, \dot{\mathbf{u}}_n^h$ and $\dot{\mathbf{u}}_{n+1}^h$.

In [36], the generalised- α method is given as

$$\mathbf{u}_{n+1}^h = \mathbf{u}_n^h + \Delta t(1 - \gamma^f)\dot{\mathbf{u}}_n^h + \Delta t\gamma^f\dot{\mathbf{u}}_{n+1}^h, \quad (25)$$

$$\mathbf{u}_{n+\alpha_f^f}^h = (1 - \alpha_f^f)\mathbf{u}_n^h + \alpha_f^f\mathbf{u}_{n+1}^h, \quad (26)$$

$$\dot{\mathbf{u}}_{n+\alpha_m^f}^h = (1 - \alpha_m^f)\dot{\mathbf{u}}_n^h + \alpha_m^f\dot{\mathbf{u}}_{n+1}^h, \quad (27)$$

where γ^f , α_m^f and α_f^f are integration parameters. These equations can be rewritten as

$$\mathbf{u}_{n+\alpha_f^f}^h = (1 - \alpha_f^f)\mathbf{u}_n^h + \alpha_f^f\mathbf{u}_{n+1}^h, \quad (28)$$

$$\dot{\mathbf{u}}_{n+\alpha_m^f}^h = \left(1 - \frac{\alpha_m^f}{\gamma^f}\right)\dot{\mathbf{u}}_n^h + \frac{\alpha_m^f}{\Delta t\gamma^f}(\mathbf{u}_{n+1}^h - \mathbf{u}_n^h), \quad (29)$$

$$\dot{\mathbf{u}}_{n+1}^h = \frac{1}{\Delta t\gamma^f}(\mathbf{u}_{n+1}^h - \mathbf{u}_n^h) - \frac{1 - \gamma^f}{\gamma^f}\dot{\mathbf{u}}_n^h. \quad (30)$$

In G_{Gal} and G_{stab} , given, respectively, by the relations (16) and (17), the expressions \mathbf{u}^h and $\dot{\mathbf{u}}^h$ are now replaced by $\mathbf{u}_{n+\alpha_f^f}^h$ and $\dot{\mathbf{u}}_{n+\alpha_m^f}^h$, respectively. Thus, the fluid velocity and its time derivative in (15) are expressed exclusively in terms of the unknown \mathbf{u}_{n+1}^h and in terms of the quantities \mathbf{u}_n^h and $\dot{\mathbf{u}}_n^h$, which are known from the solution at the previous time instant. Due to its nature as Lagrangian multiplier, which enforces continuity of the flow, the pressure should not be subjected to a time inte-

gration scheme, but be computed independently for each time increment. Once \mathbf{u}_{n+1}^h has been computed, the quantity $\dot{\mathbf{u}}_{n+1}^h$ can be obtained from (30).

The integration parameters are reduced to one independent control variable as follows:

$$\gamma^f = \frac{1}{2} + \alpha_m^f - \alpha_f^f, \quad \alpha_m^f = \frac{1}{2} \frac{3 - \rho_\infty^f}{1 + \rho_\infty^f}, \quad \alpha_f^f = \frac{1}{1 + \rho_\infty^f}, \tag{31}$$

where ρ_∞^f has to be chosen such that $0 \leq \rho_\infty^f \leq 1$. For $\rho_\infty^f = 1$, the method is identical to the trapezoidal rule, whereas the numerical damping of the method increases with smaller values of ρ_∞^f . For a detailed study of the generalised- α method in combination with stabilised finite elements we refer to [37].

6.2. Solid solver

Similarly to Section 6.1, the quantities $\mathbf{d}_n^h, \dot{\mathbf{d}}_n^h$ and $\ddot{\mathbf{d}}_n^h, n = 0, 1, \dots, N_{\text{time}}$ are introduced. For the time integration of the finite element formulation of the structure (23), we then employ the generalised- α method as presented by Chung and Hulbert in [35] for the second order initial value problems.

Thus, we define

$$\mathbf{d}_{n+1} = \mathbf{d}_n + \Delta t \dot{\mathbf{d}}_n + \Delta t^2 \left(\left(\frac{1}{2} - \beta^s \right) \ddot{\mathbf{d}}_n + \beta^s \ddot{\mathbf{d}}_{n+1} \right), \tag{32}$$

$$\dot{\mathbf{d}}_{n+1} = \dot{\mathbf{d}}_n + \Delta t \left((1 - \gamma^s) \ddot{\mathbf{d}}_n + \gamma^s \ddot{\mathbf{d}}_{n+1} \right), \tag{33}$$

$$\mathbf{d}_{n+\alpha_f^s} = (1 - \alpha_f^s) \mathbf{d}_n + \alpha_f^s \mathbf{d}_{n+1}, \tag{34}$$

$$\dot{\mathbf{d}}_{n+\alpha_f^s} = (1 - \alpha_f^s) \dot{\mathbf{d}}_n + \alpha_f^s \dot{\mathbf{d}}_{n+1}, \tag{35}$$

$$\ddot{\mathbf{d}}_{n+\alpha_m^s} = (1 - \alpha_m^s) \ddot{\mathbf{d}}_n + \alpha_m^s \ddot{\mathbf{d}}_{n+1}, \tag{36}$$

where $\mathbf{d}_{n+\alpha_f^s}, \dot{\mathbf{d}}_{n+\alpha_f^s}, \ddot{\mathbf{d}}_{n+\alpha_m^s}$, are the quantities to be employed in (23).

Similarly to the velocity \mathbf{u}_{n+1}^h in Section 6.1, one unknown kinematical quantity associated with time instant t_{n+1} can be chosen as the only independent variable. Eqs. (32)–(36) can then be rewritten to express all other kinematical data at the time instants $t_{n+1}, t_{n+\alpha_m^s}$ and $t_{n+\alpha_f^s}$ in terms of this primary unknown and the known solution at t_n . In the context of solid mechanics, it is common to employ the displacements \mathbf{d}_{n+1}^h as primary unknowns, but it is equally straightforward to rephrase (32)–(36) to render expressions in terms of the velocity $\dot{\mathbf{d}}_{n+1}^h$.

Chung and Hulbert [35] have shown that, for linear problems, the following formula for the time integration parameters is optimal

$$\begin{aligned} \beta^s &= \frac{1}{4} (1 + \alpha_m^s - \alpha_f^s)^2, & \gamma^s &= \frac{1}{2} + \alpha_m^s - \alpha_f^s, \\ \alpha_f^s &= \frac{1}{1 + \rho_\infty^s}, & \alpha_m^s &= \frac{2 - \rho_\infty^s}{1 + \rho_\infty^s}. \end{aligned} \tag{37}$$

Similarly to (31), the scalar ρ_∞^s can be identified as the spectral radius associated with infinitely large time steps and has to be chosen by the user such that $0 \leq \rho_\infty^s \leq 1$. Note that (37) differs from (31).

6.3. Mesh update

It still remains to discretise the movement of the fluid mesh in time. Therefore, the configuration $\hat{\mathbf{x}}_n^h$ and the velocity field $\hat{\mathbf{v}}_n^h$ at the discrete time instants $t_n, n = 0, 1, 2, \dots, N_{\text{time}}$ are introduced. In this work, $\hat{\mathbf{x}}_n^h$ and $\hat{\mathbf{v}}_n^h$ are related by a simple generalised midpoint scheme

$$\hat{\mathbf{v}}_{n+1}^h = \frac{1}{\Delta t \gamma^m} (\hat{\mathbf{x}}_{n+1}^h - \hat{\mathbf{x}}_n^h) - \frac{1 - \gamma^m}{\gamma^m} \hat{\mathbf{v}}_n^h, \tag{38}$$

where γ^m is an integration parameter to be chosen such that $\frac{1}{2} \leq \gamma^m \leq 1$. In this work, we set $\gamma^m = \gamma^f$ (see (31)₁), and thus make it dependent on ρ_∞^f . The following expressions are then employed in the weak form (15)

$$\hat{\mathbf{x}}_{n+\alpha_f^f}^h = (1 - \alpha_f^f) \hat{\mathbf{x}}_n^h + \alpha_f^f \hat{\mathbf{x}}_{n+1}^h, \tag{39}$$

$$\hat{\mathbf{v}}_{n+\alpha_f^f}^h = (1 - \alpha_f^f) \hat{\mathbf{v}}_n^h + \alpha_f^f \hat{\mathbf{v}}_{n+1}^h, \tag{40}$$

where α_f^f is given by (31)₃. The vector field $\hat{\mathbf{x}}_{n+\alpha_f^f}^h$ defines the configuration, which is employed in the computation of the integrals in (15).

Importantly, the mesh update strategy discussed in Section 4.1 is applied to the position of the internal nodes of the finite element mesh at t_{n+1} . In the context of a mesh update algorithm based on a quality criteria like (19), the mesh configuration given by $\hat{\mathbf{x}}_{n+\alpha_f}^h$ therefore becomes an interpolant between two “optimal” configurations.

7. Modelling of the interface and formulation of the overall problem

Prior to further discussion, it is convenient to introduce a notational representation for the unknown quantities associated with the finite element nodes of the fluid and the solid meshes. Thus, we define

$$\begin{aligned}
 & \mathbf{u}^{f-s}: \text{nodal values of the fluid velocity } \mathbf{u}^h \text{ on } \Gamma_{f-s}, \\
 \tilde{\mathbf{u}}^f = \{ & \mathbf{u}^f, \mathbf{p} \}: \text{all nodal values of } \mathbf{u}^h \text{ except those already in } \mathbf{u}^{f-s} \\
 & \text{and all nodal values of the fluid pressure } p^h, \\
 \hat{\mathbf{v}}^{f-s}: & \text{nodal values of the mesh velocity } \hat{\mathbf{v}}^h \text{ on } \Gamma_{f-s}, \\
 \hat{\mathbf{v}}^f: & \text{all nodal values of } \hat{\mathbf{v}}^h \text{ except those in } \hat{\mathbf{v}}^{f-s}, \\
 \hat{\mathbf{x}}^{f-s}: & \text{positions of the fluid nodes on interface boundary } \Gamma_{f-s} \\
 & \text{associated with fluid mesh configuration } \hat{\mathbf{x}}^h, \\
 \hat{\mathbf{x}}^f: & \text{positions of all fluid nodes subjected to mesh moving} \\
 & \text{algorithm (Section 4.1),} \\
 \mathbf{d}^{s-f}: & \text{nodal values of the translational structural} \\
 & \text{displacements in } \mathbf{d}^h \text{ on } \Gamma_{s-f}, \\
 \mathbf{d}^s: & \text{all nodal values of } \mathbf{d}^h \text{ except those already in } \mathbf{d}^{s-f} \\
 & \text{and, if relevant, all rotational degrees of freedom} \\
 & \text{of the structure.}
 \end{aligned} \tag{41}$$

7.1. Kinematic consistency of the discretised interface

After the spatial and temporal discretisation of the fluid flow and the solid structure in the previous sections the remaining task is to link the fluid and the structural finite element meshes along the interface boundary, such that the boundary conditions (7)–(9), (13) and (14) are satisfied with sufficient accuracy.

In order to resolve the complex fluid flow in the boundary layer most practical applications require the discretisation of the fluid domain near the interface to be denser than that of the structure. Consequently, the kinematics of the interface is typically determined by the discretisation of the surface of the solid structure. Therefore, in order to satisfy the kinematic boundary conditions along the interface we have chosen a simple interpolation strategy based on the finite element discretisation of the solid structure.

It then follows (see Fig. 1) that the boundary conditions (7), (8) and (13) may be satisfied by introducing the discrete counterparts of Eqs. (22) and (21), respectively, as

$$\hat{\mathbf{x}}_A^{f-s} = \mathcal{J}_A(\mathbf{x}_{B,0}^{s-f} + \mathbf{d}_B^{s-f}) = \sum_{B=1}^{M^s} c_{B,A}(\mathbf{x}_{B,0}^{s-f} + \mathbf{d}_B^{s-f}), \tag{42}$$

$$\mathbf{u}_A^{f-s} = \hat{\mathbf{v}}_A^{f-s} = \mathcal{J}_A(\dot{\mathbf{d}}_B^{s-f}) = \sum_{B=1}^{M^s} c_{B,A} \dot{\mathbf{d}}_B^{s-f} \tag{43}$$

and, consequently,

$$\dot{\mathbf{u}}_A^{f-s} = \mathcal{J}_A(\ddot{\mathbf{d}}_B^{s-f}) = \sum_{B=1}^{M^s} c_{B,A} \ddot{\mathbf{d}}_B^{s-f}, \tag{44}$$

where $\mathcal{J}_A(\bullet)$ is the transfer operator, introduced in (21) and (22), for fluid node A . In Eqs. (42)–(44), the number of solid nodes which describe one face or edge of a structural element is denoted by M^s . Thus, we have $M^s = 2$ for quadrilateral two-dimensional continuum elements or $M^s = 4$ for three-dimensional brick elements. The vectors $\hat{\mathbf{x}}_A^{f-s}$, \mathbf{u}_A^{f-s} , $\hat{\mathbf{v}}_A^{f-s}$ and $\dot{\mathbf{u}}_A^{f-s}$ are associated with node A of the fluid mesh. Similarly, \mathbf{d}_B^{s-f} , $\dot{\mathbf{d}}_B^{s-f}$ and $\ddot{\mathbf{d}}_B^{s-f}$ are the displacement, velocity and acceleration of the solid finite element node B at the interface boundary. The vector $\mathbf{x}_{B,0}^{s-f}$ denotes the initial position of the structural node B . The coefficient $c_{B,A} = N_B^s(\zeta_A)$ represents the value of the structural shape function associated with node B and evaluated

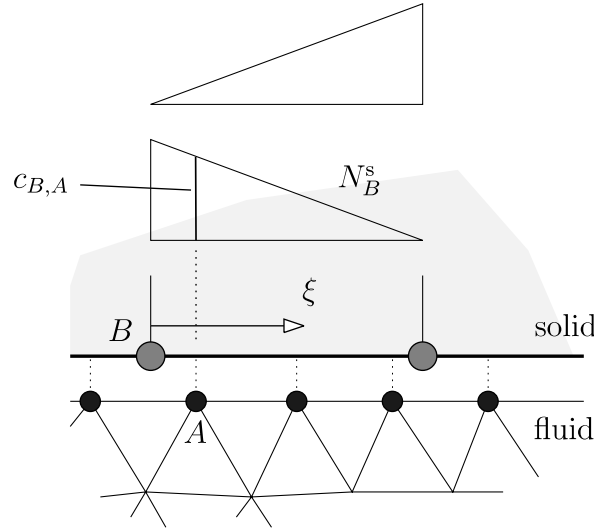


Fig. 1. Fluid–solid interface, interpolation of data based on the finite element discretisation of the solid structure.

at the position of the fluid node A , as shown in Fig. 1. We note that within the strategy described in this work the coefficients $c_{B,A}$ do not change throughout the simulation.

It is shown later in Section 7.2 that the introduction of the kinematical relations (42)–(44) into the combined weak form of the overall problem leads to implicit fulfilment of the traction boundary conditions (9) and (14).

The choice of a slightly different time integration scheme for the fluid and the structure, as discussed in Section 6, is incorporated into the interface kinematics by requiring the Eqs. (42)–(44) to hold at the discrete time instants t_n, t_{n+1}, \dots . As a consequence of this, the quantities $\mathbf{u}_{n+\alpha_f}^{f-s}, \hat{\mathbf{v}}_{n+\alpha_f}^{f-s}$ and $\mathbf{d}_{n+\alpha_f}^{s-f}$, which represent linear interpolations of the velocities at the time instants t_n and t_{n+1} , do not necessarily satisfy the condition (43) exactly. The same applies to the interpolated nodal positions and accelerations. The authors have not experienced any numerical problems associated with this small inconsistency.

7.2. Coupled overall problem

For notational convenience, we henceforth define the representation of the nodal quantities in (41) to be associated with the time instant t_{n+1} . By combining the equations presented in the previous sections, the complete discrete problem may then be expressed as follows: For any variation $\delta \mathbf{d}^{s-f}, \delta \mathbf{d}^s$ and $\delta \tilde{\mathbf{u}}^f$, find $\mathbf{d}^{s-f}, \mathbf{d}^s, \tilde{\mathbf{u}}^f, \hat{\mathbf{x}}^f$, such that

$$\tilde{G}_{\text{Gal+stab}}^f(\tilde{\mathbf{u}}^f, \mathbf{u}^{f-s}(\mathbf{d}^{s-f}), \hat{\mathbf{x}}^f, \hat{\mathbf{x}}^{f-s}(\mathbf{d}^{s-f}); \delta \tilde{\mathbf{u}}^f, \delta \mathbf{d}^{s-f}) + \tilde{G}^s(\mathbf{d}^s, \mathbf{d}^{s-f}; \delta \mathbf{d}^s, \delta \mathbf{d}^{s-f}) = 0, \quad (45)$$

$$\tilde{\mathbf{m}}(\hat{\mathbf{x}}^f, \hat{\mathbf{x}}^{f-s}(\mathbf{d}^{s-f})) = \mathbf{0}. \quad (46)$$

Eq. (45) represents the combined weak forms (15) and (23), whereas the system of equation (46) is based on one of the mesh update procedures discussed in Section 4.1. The relations given by the time integration scheme in Section 6 have been employed to eliminate $\hat{\mathbf{v}}^{f-s}, \hat{\mathbf{v}}^f, \hat{\mathbf{u}}^{f-s}, \hat{\mathbf{u}}^f, \mathbf{d}^{s-f}, \mathbf{d}^s, \mathbf{d}^{s-f}$ and \mathbf{d}^s associated with t_{n+1} as well as all kinematical data interpolated between the two time instants t_n and t_{n+1} . The equations given in Section 6.2 are also implicitly included in the terms $\tilde{G}^s(\mathbf{d}^s, \mathbf{d}^{s-f}; \delta \mathbf{d}^s, \delta \mathbf{d}^{s-f})$ and $\hat{\mathbf{x}}^{f-s}(\mathbf{d}^{s-f})$ to recover the structural displacements at the interface \mathbf{d}^{s-f} from the velocities \mathbf{d}^{s-f} .

After the elimination of the variational quantities, Eq. (45) may be rewritten in terms of nodal forces $\{\tilde{\mathbf{g}}^f, \mathbf{g}^{f-s}\}$ and $\{\mathbf{g}^s, \mathbf{g}^{s-f}\}$ associated, respectively, with the weak forms of the fluid and the solid. Thus, we obtain

$$\tilde{\mathbf{g}}^f(\tilde{\mathbf{u}}^f, \mathbf{u}^{f-s}(\mathbf{d}^{s-f}), \hat{\mathbf{x}}^f, \hat{\mathbf{x}}^{f-s}(\mathbf{d}^{s-f})) = \mathbf{0}, \quad (47)$$

$$\sum_{A=1}^{M^f} \mathbf{g}_A^{f-s}(\tilde{\mathbf{u}}^f, \mathbf{u}^{f-s}(\mathbf{d}^{s-f}), \hat{\mathbf{x}}^f, \hat{\mathbf{x}}^{f-s}(\mathbf{d}^{s-f})) c_{B,A} + \mathbf{g}_B^{s-f}(\mathbf{d}^s, \mathbf{d}^{s-f}) = \mathbf{0}, \quad (48)$$

$$\mathbf{g}^s(\mathbf{d}^s, \mathbf{d}^{s-f}) = \mathbf{0}, \quad (49)$$

whereby (48) applies to every structural node B on the interface boundary of the solid mesh and M^f is the fluid counterpart of M^s . The discrete relation (48) corresponds to the principle of virtual work applied to the nodal forces \mathbf{g}^{f-s} and \mathbf{g}^{s-f} and is based on the kinematics of the interface boundary of the structural finite element mesh. Thus, the boundary conditions (9) and (14) are satisfied in a weak sense, similar to the treatment of any standard von Neumann boundary condition in the

finite element framework. More information on the transfer of kinematical data and forces across the fluid–structure interface is given in e.g. [47].

We finally introduce the following compact representation of the overall problem

$$\mathbf{g}^f(\tilde{\mathbf{u}}^f, \tilde{\mathbf{x}}^f, \tilde{\mathbf{d}}^{s-f}) = \mathbf{0}, \quad n^f = (N^f \times (n_{\text{dim}} + 1) + N^{f-s}), \quad (50)$$

$$\mathbf{g}^i(\tilde{\mathbf{u}}^f, \tilde{\mathbf{x}}^f, \tilde{\mathbf{d}}^{s-f}, \mathbf{d}^s) = \mathbf{0}, \quad n^i = (N^{s-f} \times n_{\text{dim}}), \quad (51)$$

$$\mathbf{g}^s(\mathbf{d}^s, \tilde{\mathbf{d}}^{s-f}) = \mathbf{0}, \quad n^s = (N^s \times (n_{\text{dim}} + m) + N^s \times m), \quad (52)$$

$$\mathbf{m}(\tilde{\mathbf{x}}^f, \tilde{\mathbf{d}}^{s-f}) = \mathbf{0}, \quad n^m = (N^f \times n_{\text{dim}}), \quad (53)$$

where the numbers of scalar equations, which constitute the systems (50)–(53), are given as n^f , n^i , n^s and n^m , respectively identifying the number of degrees of freedom of the fluid, the interface, the structure and the fluid mesh. In the above set of equations, the relations (47)–(49) have been rewritten, respectively, as (50)–(52), whereby the vector \mathbf{g}^i denotes the combined nodal residual forces on the fluid–structure interface. The mesh update (46) is represented by Eq. (53). The integers N^f and N^s , N^{f-s} and N^{s-f} denote, respectively, the numbers of internal nodes and the numbers of interface boundary nodes of the fluid and the solid meshes. The space dimension is given by n_{dim} . Furthermore, we allow for m degrees of freedom per structural finite element node in addition to the n_{dim} translational displacements. Such degrees of freedom may include structural rotations or temperatures, which are not directly coupled with the fluid flow at the interface. Note that, similarly, the fluid pressure is not transferred explicitly across the interface since its effect on the structural deformation is accounted for by the transfer of the nodal forces via Eq. (51). In the subsystems (50), (52) and (53), the numbers of equations may change due to eventual standard Dirichlet boundary conditions or due to prescribed Eulerian areas of the fluid mesh. Clearly, the systems (50)–(53) are strongly coupled and highly non-linear.

7.3. Extension to a more general and modular framework

At the outset, the derivation of system (50)–(53) was based on identifying the kinematics of the interface with the discretisation of the structural surface. However, the coupled system (50)–(53) may also be obtained from a more generic framework based on the introduction of an independent discretisation of the interface, as shown schematically in Fig. 2. The kinematical ‘interface degrees’ of freedom, which we represent by the vector \mathbf{u}^i , can then be linked with both the fluid and the solid, similarly to the solid-to-fluid interpolation outlined above. The relations between the fluid, the solid and the independent interface are illustrated in Fig. 3. In this case the expression $\tilde{\mathbf{d}}^{s-f}$ in (50)–(53) has to be replaced by \mathbf{u}^i .

We note that this extended framework does not depend on the structural discretisation being coarser than that of the fluid domain. It allows a more modular computer implementation and thus facilitates future extensions of the methodology. Such extensions may include, for instance, independent remeshing of the fluid or the solid domains. It may also prove useful to employ a ‘mortar’ or related methodologies (see e.g. [48–50]) for the data transfer between the adjacent phases. This can be incorporated into the framework described in this work by defining a more elaborate mapping operator $\mathcal{S}(\bullet)$.

Furthermore, it is pointed out that the computational cost of solving (50)–(53) depends significantly on the number of ‘interface degrees’ of freedom. In many cases, the choice of a coarse independent interface discretisation may thus allow to obtain a good computational model of the fluid–structure interaction at low computational cost.

Finally, the introduction of independent interface degrees of freedom facilitates the application of the computational framework to different physical problems such as fluid–rigid body interaction or free surface flow (see [3–5]).

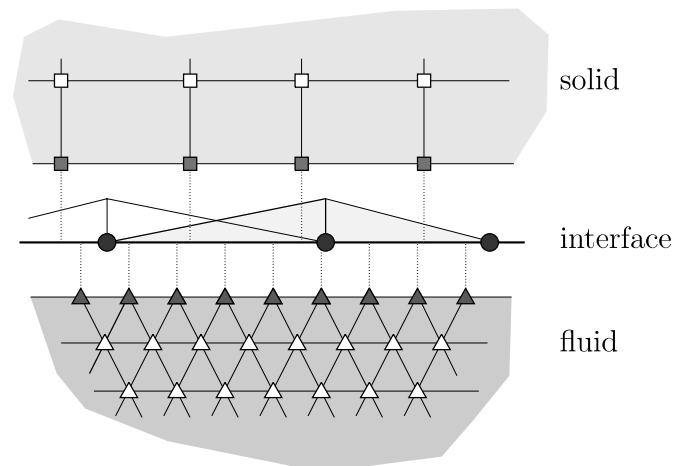


Fig. 2. General interface modelling, transfer based on finite element type interpolation of the interface domain.

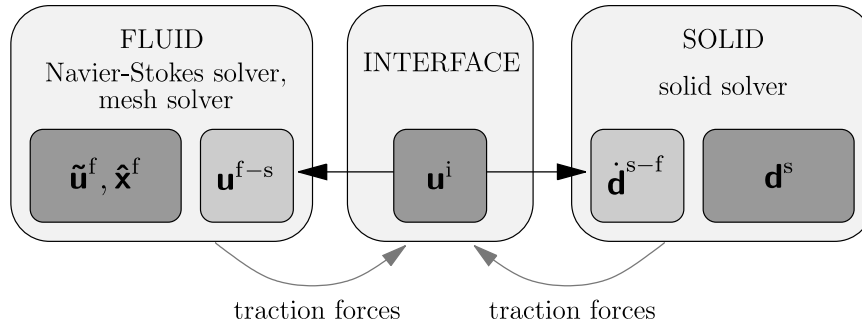


Fig. 3. Domain decomposition based on introduction of interface d.o.f. \mathbf{u}^i .

8. Solution algorithm

Given the solution at the time instant t_n , the non-linear coupled system (50)–(53) has to be solved for $\tilde{\mathbf{u}}^f, \hat{\mathbf{x}}^f, \mathbf{d}^s$ and \mathbf{u}^i at the next time instant t_{n+1} . The solution strategy developed in the course of this work is essentially based on the Newton–Raphson method.

The methodology can briefly be described as follows: On the basis of the solution at t_n an initial guess is made for $\tilde{\mathbf{u}}^f$ and \mathbf{u}^i at t_{n+1} . Next, the positions of the fluid nodes $\hat{\mathbf{x}}^f$ and the internal degrees of freedom \mathbf{d}^s of the structure are adjusted to the new configuration of the interface as given by \mathbf{u}^i (fluid mesh solver (53) and structural solver (52)). The derivatives $\partial \hat{\mathbf{x}}^f / \partial \mathbf{u}^i$ and $\partial \mathbf{d}^s / \partial \mathbf{u}^i$ are computed. Subsequently, the residual forces \mathbf{g}^f and \mathbf{g}^i are evaluated. If the tolerances are met, then the procedure can be aborted to proceed with the next time step. Otherwise, the linearisations of \mathbf{g}^f and \mathbf{g}^i with respect to the unknowns $\tilde{\mathbf{u}}^f$ and \mathbf{u}^i are computed. To this end, all partial derivatives of \mathbf{g}^f and \mathbf{g}^i are calculated and, by following the chain rule, reduced to the exact derivatives with respect to $\tilde{\mathbf{u}}^f$ and \mathbf{u}^i . The linearisations of \mathbf{g}^f and \mathbf{g}^i can then be solved for the increments of $\tilde{\mathbf{u}}^f$ and \mathbf{u}^i (combined fluid + interface solver). The unknowns are updated, and the complete procedure is repeated for the improved values of $\tilde{\mathbf{u}}^f$ and \mathbf{u}^i .

A summary of the algorithm is given in Box 1. Henceforth, the execution of steps 1–7 is referred to as one ‘overall Newton step’.

In the following, some implementation details of the algorithm are discussed. The numbering of the comments refers to the steps given in Box 1.

Box 1: Partitioned Newton–Raphson procedure to solve the system (50)–(53)

1. estimate $\tilde{\mathbf{u}}^f, \mathbf{u}^i$
2. fluid mesh solver $\mathbf{m}(\hat{\mathbf{x}}^f, \mathbf{u}^i) = \mathbf{0}$
 - (a) compute $\hat{\mathbf{x}}^f$ on the basis of \mathbf{u}^i
 - (b) compute $\frac{\partial \hat{\mathbf{x}}^f}{\partial \mathbf{u}^i}$ from $\frac{\partial \mathbf{m}}{\partial \hat{\mathbf{x}}^f} \frac{\partial \hat{\mathbf{x}}^f}{\partial \mathbf{u}^i} = -\frac{\partial \mathbf{m}}{\partial \mathbf{u}^i}$
3. solid solver $\mathbf{g}^s(\mathbf{d}^s, \mathbf{u}^i) = \mathbf{0}$
 - (a) compute \mathbf{d}^s on the basis of \mathbf{u}^i
 - (b) compute $\frac{\partial \mathbf{d}^s}{\partial \mathbf{u}^i}$ from $\frac{\partial \mathbf{g}^s}{\partial \mathbf{d}^s} \frac{\partial \mathbf{d}^s}{\partial \mathbf{u}^i} = -\frac{\partial \mathbf{g}^s}{\partial \mathbf{u}^i}$
4. compute residuals $\mathbf{g}^f(\tilde{\mathbf{u}}^f, \hat{\mathbf{x}}^f, \mathbf{u}^i), \mathbf{g}^i(\tilde{\mathbf{u}}^f, \hat{\mathbf{x}}^f, \mathbf{u}^i, \mathbf{d}^s)$,
if $\mathbf{g}^f, \mathbf{g}^i < \text{tol}$, then exit
5. compute derivatives

$$\mathbf{A} = \frac{\partial \mathbf{g}^f}{\partial \tilde{\mathbf{u}}^f}, \quad \mathbf{B} = \frac{\partial \mathbf{g}^f}{\partial \mathbf{u}^i} + \frac{\partial \mathbf{g}^f}{\partial \hat{\mathbf{x}}^f} \frac{\partial \hat{\mathbf{x}}^f}{\partial \mathbf{u}^i}$$

$$\mathbf{C} = \frac{\partial \mathbf{g}^i}{\partial \tilde{\mathbf{u}}^f}, \quad \mathbf{D} = \frac{\partial \mathbf{g}^i}{\partial \mathbf{u}^i} + \frac{\partial \mathbf{g}^i}{\partial \hat{\mathbf{x}}^f} \frac{\partial \hat{\mathbf{x}}^f}{\partial \mathbf{u}^i} + \frac{\partial \mathbf{g}^i}{\partial \mathbf{d}^s} \frac{\partial \mathbf{d}^s}{\partial \mathbf{u}^i}$$
6. solve combined fluid + interface solver

$$\begin{bmatrix} \mathbf{A} & \mathbf{B} \\ \mathbf{C} & \mathbf{D} \end{bmatrix} \begin{Bmatrix} \Delta \tilde{\mathbf{u}}^f \\ \Delta \mathbf{u}^i \end{Bmatrix} = -\begin{Bmatrix} \mathbf{g}^f \\ \mathbf{g}^i \end{Bmatrix}, \quad \begin{Bmatrix} \tilde{\mathbf{u}}^f \\ \mathbf{u}^i \end{Bmatrix} \leftarrow \begin{Bmatrix} \tilde{\mathbf{u}}^f \\ \mathbf{u}^i \end{Bmatrix} + \begin{Bmatrix} \Delta \tilde{\mathbf{u}}^f \\ \Delta \mathbf{u}^i \end{Bmatrix}$$
7. goto 2.

1. At the beginning of each time step, the solution at the previous time instant can be employed as the initial guess for $\tilde{\mathbf{u}}^f$ and \mathbf{u}^i . An improved guess may be obtained by employing a more sophisticated extrapolation in time based on the previous solutions. Note, however, that, in the examples presented in Section 9, such strategies have rarely led to better performance of the overall scheme. This proves the high degree of non-linearity of the problems considered, and also suggests the restriction of explicit solution techniques to small time steps.
2. In this step, the nodal positions $\hat{\mathbf{x}}^f$ of the fluid mesh are adjusted to the new configuration of the rigid body (see Sections 4.2 and 4.1). The mesh update strategies discussed in Section 4.1 are non-linear and thus, a Newton–Raphson procedure is employed. Once $\hat{\mathbf{x}}^f$ has been computed such that $\mathbf{m}(\hat{\mathbf{x}}^f, \mathbf{u}^i) = \mathbf{0}$, we may write, for small $d\hat{\mathbf{x}}^f$ and $d\mathbf{u}^i$,

$$\frac{\partial \mathbf{m}}{\partial \hat{\mathbf{x}}^f} d\hat{\mathbf{x}}^f + \frac{\partial \mathbf{m}}{\partial \mathbf{u}^i} d\mathbf{u}^i = \mathbf{0} \quad (54)$$

and consequently,

$$\frac{\partial \mathbf{m}}{\partial \hat{\mathbf{x}}^f} \frac{\partial \hat{\mathbf{x}}^f}{\partial \mathbf{u}^i} = - \frac{\partial \mathbf{m}}{\partial \mathbf{u}^i}. \quad (55)$$

Thus, the i th column of the derivative matrix $\partial \hat{\mathbf{x}}^f / \partial \mathbf{u}^i$ can be obtained from a system of linear equations, where the i th column of $-\partial \mathbf{m} / \partial \mathbf{u}^i$ is used as the right hand side vector. The matrix $\partial \mathbf{m} / \partial \hat{\mathbf{x}}^f$ coincides with the linearisation matrix from the last step of the Newton procedure used to determine $\hat{\mathbf{x}}^f$ for the given \mathbf{u}^i . Thus, conveniently, the LU-decomposition of $\partial \mathbf{m} / \partial \hat{\mathbf{x}}^f$ is still available. The derivative $\partial \hat{\mathbf{x}}^f / \partial \mathbf{u}^i$ is then obtained from a simple backward and forward substitution for different right hand sides. Importantly, by applying this strategy, no inverse matrices need to be assembled, and costly matrix multiplication is avoided.

For larger problems, the computational cost involved in these operations is dominated by the repeated backward and forward substitutions. Thus, it is proportional to the number of columns in $\partial \hat{\mathbf{x}}^f / \partial \mathbf{u}^i$ and $\partial \mathbf{m} / \partial \mathbf{u}^i$, which corresponds to the number of degrees of freedom of the discretised interface n^i .

3. The actions to be taken in this step are very similar to those in step 2. In the solid solver, we compute \mathbf{d}^s on the basis of the current \mathbf{u}^i by means of a Newton–Raphson procedure such that (52) is satisfied and, subsequently, we employ the structural stiffness matrix of the last Newton step to compute the derivative $\partial \mathbf{d}^s / \partial \mathbf{u}^i$ from the relation

$$\frac{\partial \mathbf{g}^s}{\partial \mathbf{d}^s} \frac{\partial \mathbf{d}^s}{\partial \mathbf{u}^i} = - \frac{\partial \mathbf{g}^s}{\partial \mathbf{u}^i}. \quad (56)$$

Similarly to step 2, the computational cost associated with the backward and forward substitutions is proportional to the number of degrees of freedom of the interface n^i .

4. This step requires the evaluation of the residuals \mathbf{g}^f and \mathbf{g}^i . If the tolerances are met, then solution at time instant t_{n+1} is given by the current values of $\tilde{\mathbf{u}}^f$, $\hat{\mathbf{x}}^f$, \mathbf{d}^s and \mathbf{u}^i . One can then proceed with the next time step.
5. The partial derivatives of the residual vectors \mathbf{g}^f and \mathbf{g}^i with respect to $\tilde{\mathbf{u}}^f$, $\hat{\mathbf{x}}^f$, \mathbf{d}^s and \mathbf{u}^i are computed. Following the chain rule, the derivatives $\partial(\bullet) / \partial \hat{\mathbf{x}}^f$ and $\partial(\bullet) / \partial \mathbf{d}^s$ are multiplied by the matrices $\partial \hat{\mathbf{x}}^f / \partial \mathbf{u}^i$ and $\partial \mathbf{d}^s / \partial \mathbf{u}^i$, respectively. The exact linearisation of the combined residual vector $\{\mathbf{g}^f, \mathbf{g}^i\}$ with respect to the unknowns $\tilde{\mathbf{u}}^f$ and \mathbf{u}^i is then fully defined. The numbers of scalar multiplications required for the matrix operations are obtained as

$$\frac{\partial \mathbf{g}^f}{\partial \hat{\mathbf{x}}^f} \frac{\partial \hat{\mathbf{x}}^f}{\partial \mathbf{u}^i} \rightarrow n^f \times n^m \times n^i, \quad (57)$$

$$\frac{\partial \mathbf{g}^i}{\partial \hat{\mathbf{x}}^f} \frac{\partial \hat{\mathbf{x}}^f}{\partial \mathbf{u}^i} \rightarrow n^i \times n^m \times n^i, \quad (58)$$

$$\frac{\partial \mathbf{g}^i}{\partial \mathbf{d}^s} \frac{\partial \mathbf{d}^s}{\partial \mathbf{u}^i} \rightarrow n^i \times n^s \times n^i. \quad (59)$$

For a typical problem, we have $n^f > n^m > n^s > n^i$. Thus, it follows that the multiplications (58) and (59) are rather inexpensive, whereas (57) is clearly more involving. Therefore, this part of the algorithm should be implemented carefully, taking all possible advantage of the sparseness of $\partial \mathbf{g}^f / \partial \hat{\mathbf{x}}^f$.

6. The pattern of non-zero entries of a typical system matrix of the combined fluid + interface solver is displayed in Fig. 4. The pattern is almost symmetric and the degree of asymmetry depends on the number of interface degrees of freedom n^i . In this work, a direct sparse solver is employed for the solution of the linear system.

The interaction of fluid flow with a stiff structure may lead to an ill-conditioned system matrix. In such cases, a standard preconditioning technique may be employed. For the choice of the optimal strategy it should be noted that any ill-conditioning arises from the contribution of the structure to part \mathbf{D} of the matrix, which is relatively small. The matrix is regular even without the contribution of the structure. It is also pointed out, that the interaction of fluid flow with very stiff structures can be solved by means of basic iterative schemes (e.g. block Gauß–Seidel, see e.g. [40,39]). However, such strategies fail or converge poorly when applied to the interaction of fluid flow with flexible structures and large

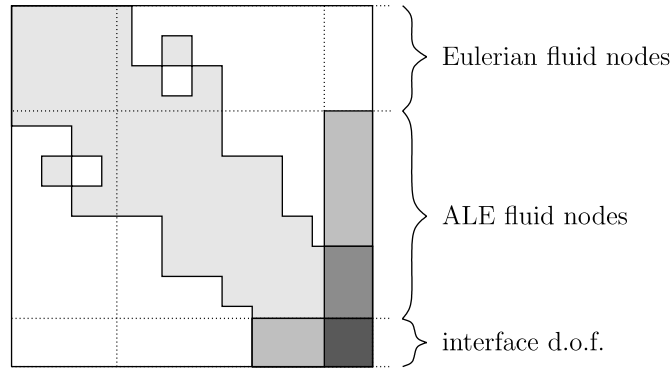


Fig. 4. Typical system matrix of the combined fluid + interface solver.

structural deformations, which is indeed the focus of this work. The solutions of the examples presented in Section 9 have been obtained without any preconditioning.

For the steps 2, 3 and 5, various element derivative matrices need to be evaluated. The derivative $\partial \mathbf{g}^f / \partial \hat{\mathbf{x}}^f$ is particularly tedious due to the formulation of (16) and (17) in the current mesh configuration. Thus, the element area and all shape function derivatives need to be linearised. However, the computation of the derivatives is considered to be a straightforward exercise and, therefore, it is not addressed any further in this work.

The computer memory needed for storing the global matrices $\partial \hat{\mathbf{x}}^f / \partial \mathbf{u}^i$ and $\partial \mathbf{d}^s / \partial \mathbf{u}^i$ is smaller than the workspace typically required by the combined fluid + interface solver. Provided an efficient computer implementation is employed and provided n^i is relatively small, the memory requirements associated with the resolution of the interaction do not exceed those of the fluid and the structural subsolvers.

Finally, we recall that the solution strategy outlined in Box 1 performs most efficiently for problems with large Eulerian parts of the fluid mesh and small numbers of structural and interface degrees of freedom, i.e. $n^m \ll n^f$, $n^s \ll n^f$, $n^i \ll n^m$, respectively. For small n^i and n^s , the proportions of computational time spent in the different steps of the algorithm resemble those associated with the solution methodology for fluid–rigid body interaction described in [4]. For problems with larger numbers of interface degrees of freedom, the computation of the derivatives in the steps 2 and 3 and the matrix multiplications in step 5 require a larger proportion of computational time. However, the optimal convergence behaviour, which results from the exact linearisation of the overall problem, may still make the methodology at hand very competitive in comparison to alternative strategies.

9. Numerical examples

9.1. Flow-induced vibration of a flexible beam

This model problem has been presented by Wall [51,19] and later by Hübner et al. [52,53] and Steindorf [54] to test their numerical solution strategies for fluid–structure interaction problems.

A fixed square rigid body is submerged in incompressible fluid flow. Far away the flow is uniform with the velocity u_∞ . A flexible thin beam is attached to the rigid body in the centre of the downstream face. In the undeformed configuration the beam is aligned with the far field flow. The vortices, which separate from the corners of the rigid body, generate lift forces which excite oscillations of the flexible beam.

The geometry and the boundary conditions are given in Fig. 5. The material parameters of the fluid and the solid are taken from Wall [19] as, respectively, $\mu^f = 1.82 \times 10^{-4}$, $\rho^f = 1.18 \times 10^{-3}$ and $\mu^s = 9.2593 \times 10^5$, $K^s = 2.78 \times 10^6$, $\rho^s = 0.1$. The shear and bulk moduli μ^s and K^s correspond to the Young’s modulus $E = 2.5 \times 10^6$ and the Poisson’s ratio $\nu = 0.35$. Plane stress conditions are assumed to hold for the solid. The inflow velocity is chosen as $u_\infty = 51.3$. Thus, the Reynolds number is obtained as $Re = \rho^f D u_\infty / \mu^f = 333$, whereby $D = 1$ is the diameter of the square rigid body.

Three different numerical representations of the flexible structure are considered: First, it is discretised with 20 nine noded and fully integrated finite elements of equal size with only one element in the thickness direction of the beam (A). We apply the plane stress condition and assume small strain elastic behaviour. This corresponds to Wall [19]. The second model (B) differs from the first only by the employment of Neo–Hooke type large strain elasticity based on the following stress–strain relation

$$\boldsymbol{\sigma} = \mu J^{-\frac{5}{3}} \left(\mathbf{B} - \frac{1}{3} \text{tr}(\mathbf{B}) \mathbf{I} \right) + K \frac{J^2 - 1}{2J} \mathbf{I}, \tag{60}$$

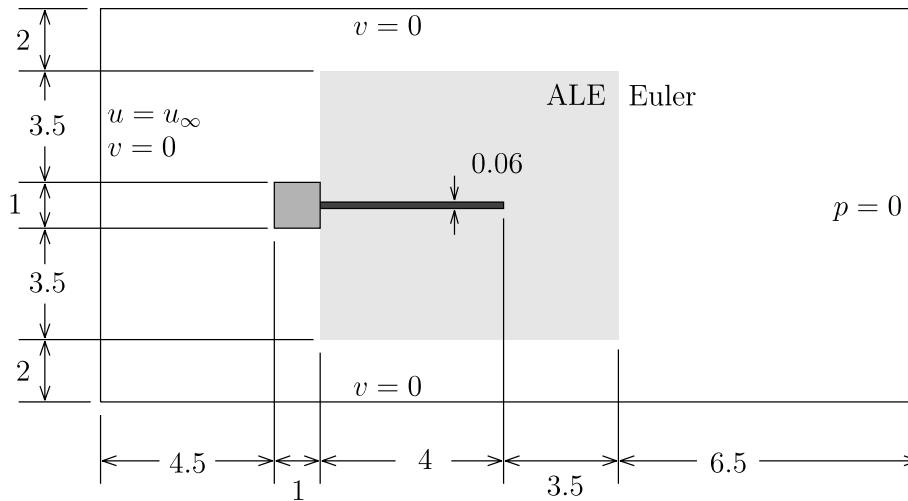


Fig. 5. Flow induced vibrations of a flexible beam: geometry and boundary conditions.

where J is the determinant of the deformation gradient \mathbf{F} , $\mathbf{B} = \mathbf{F}\mathbf{F}^T$ is the left Cauchy–Green tensor and $\boldsymbol{\sigma}$ denotes the Cauchy stress tensor. Thirdly, a representation with 20 linear geometrically exact beam elements is considered (C). The element formulation employed is described in detail in [55] and uses one-Gauß-point integration to avoid shear locking. The following parameters can be computed from the above given data: $EA = 1.5 \times 10^5$, $EI = 45.0$ and $\kappa GA = 4.63 \times 10^4$.

All translational structural degrees of freedom at the interface are employed as interface degrees of freedom. The kinematical data of the fluid at the interface is obtained from the interface degrees of freedom by linear interpolation. We note that the continuum models A and B and the beam model C of the structure render, respectively, 80 or 20 interface nodes, which shall result in a substantial difference of computational time. The employment of fewer interface nodes for the continuum models A and B is not advantageous, since it results in unwanted stiffening of the thin structure.

Since the thickness of the beam elements is neglected, different fluid meshes are needed. Therefore, three meshes with 4336, 12,330 (for the interaction with models A, B, respectively) and 4564 elements (for the interaction with model C) are generated. Details of the meshes are displayed in Fig. 6. The time integration parameters are set to $\rho_\infty^f = 0.8$ for the fluid and $\rho_\infty^s = 0.5$ for the solid structure. The update of the positions of the internal nodes of the fluid mesh is performed according to the strategy based on (19). Initially, the fluid and the structure are at rest, and at $t = 0$ the inflow velocity u_∞ is applied instantaneously. The simulations are performed for different time step sizes Δt .

The diagrams in Figs. 7–9 show the evolution of the displacement d of the tip of the flexible beam in time. Some typical flow patterns are displayed in the vorticity diagrams in Fig. 10. The convergence of the solution procedure is demonstrated in Tables 1 and 2.

The following observations are made on the basis of the numerical results:

- Every simulation renders an unsteady periodic long term response of the flexible beam. The build-up of the oscillations takes approximately 2 time units. For all discretisations considered, the amplitudes of the oscillating tip displacement d lie between 1.1 and 1.4. The average frequency \bar{f} is obtained between 2.96 and 3.31. This interval contains the lowest eigenfrequency of the beam $f_1 \approx 3.03$ and also agrees well with the results obtained in [19,52,54].
- It is evident from Fig. 7 that the deviation of the responses of the structural models A, B and C is relatively small.
- Figs. 8 and 9 demonstrate that, in some cases, different temporal and spatial discretisations lead to a modulation of the oscillation of the beam tip or to the superposition with a small amplitude oscillation at a higher frequency. This is due to high frequency effects, which are resolved if the discretisation is sufficiently fine, but otherwise damped out. In fact, the second eigenfrequency of the small strain structural model corresponds to $T_2 \approx 0.053$, which is resolved by $\Delta t = 0.005$, but not by $\Delta t = 0.02$. Therefore, a conclusive study of the amplitude modulation and the high frequency effects would require very dense spatial and temporal discretisations.
- In all cases, the convergence of the absolute residuals of the combined fluid + interface solver and of the subsolvers is asymptotically quadratic. This is illustrated by Tables 1 and 2, which are associated with two specific simulations.

9.2. Flow through a channel with a flexible wall

This preliminary numerical study is motivated by the work of Pedley and co-workers [56,57]. We consider the two-dimensional flow through a channel with a flexible wall, i.e. a section of the channel wall consists of a Neo–Hooke elastic

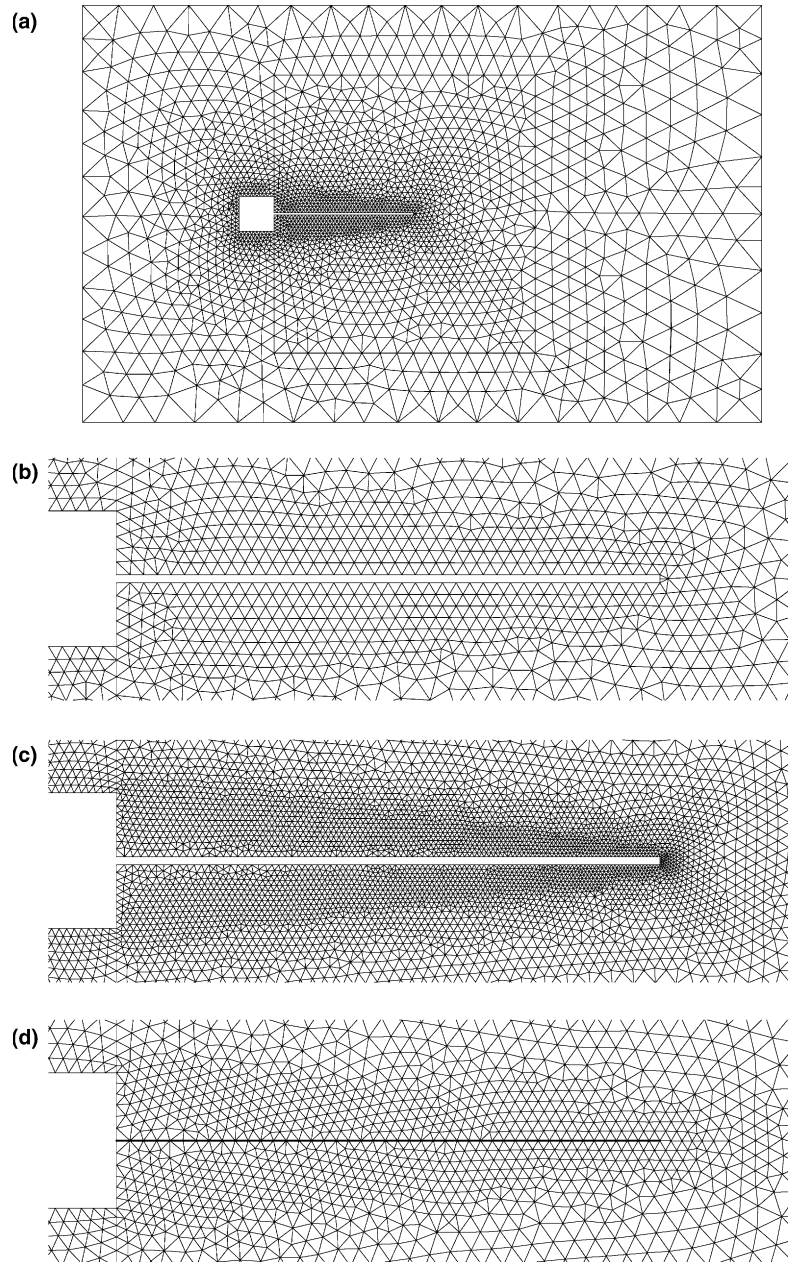


Fig. 6. Flow induced vibrations of a flexible beam: fluid finite element meshes; (a) mesh with 4336 elements, (b) detail of meshes with 4336, (c) 12,330, and (d) 4564 elements. The mesh with 4564 elements is employed for the interaction with beam elements C.

membrane, otherwise the wall is fixed in space. Similar problems arise in the area of biomechanics, where the objective is to model the blood flow through the flexible vessels in the human body.

At the inflow boundary the prescribed flow profile corresponds to undisturbed Poiseuille flow. The average inflow velocity is chosen as $\bar{u}_{in} = 1$. The geometry and the boundary conditions are given in Fig. 11. The fluid properties are set to $\mu^f = 0.002$ and $\rho^f = 1$. The Reynolds number is obtained as $Re = \bar{u}_{in} D \rho^f / \mu^f = 500$, where $D = 1$ is the width of the channel. The flexible membrane is incompressible and Neo-Hooke elastic with $\mu^s = 260$. The constitutive stress-strain relation for such material is given in one-dimension by

$$\sigma = \mu^s \frac{\lambda^4 - 1}{\lambda^2}, \tag{61}$$

where σ denotes the principal Cauchy stress associated with the in-plane stretch λ . Eq. (61) can be derived from (60) by assuming plane strain conditions and exact incompressibility ($K^s \rightarrow \infty$). The membrane is connected to the points A and B, whereby it is prestressed such that $\lambda_0 = 1.2$. The thickness of the stress-free membrane is 0.01 and the density is neglected, i.e. $\rho^s = 0$. The external pressure is set to $p_{ext} = 0.5$.

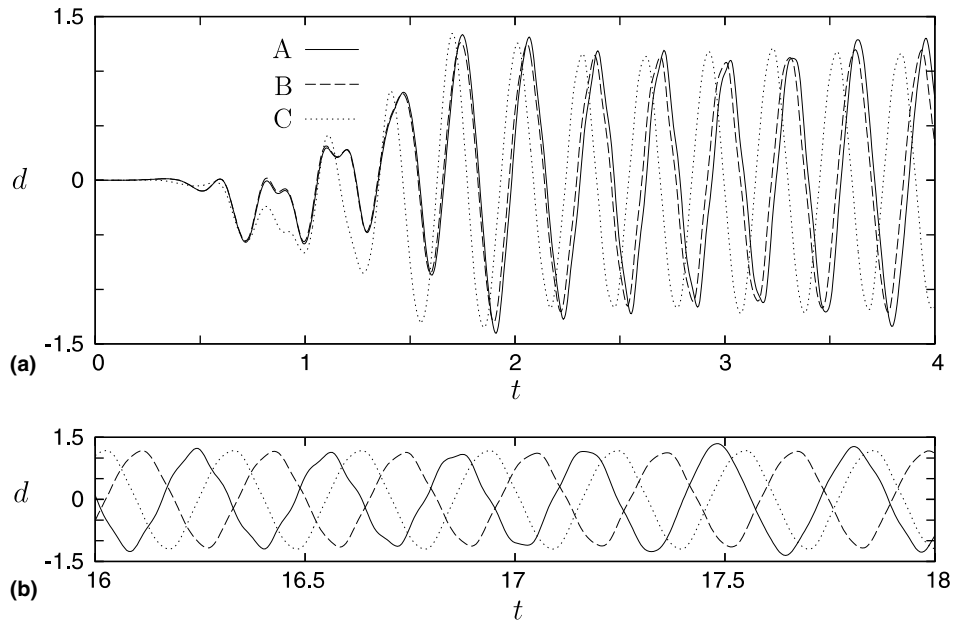


Fig. 7. Flow induced vibrations of a flexible beam: vertical displacement d of the tip of the structure; $\Delta t = 0.005$; 4336 fluid elements, 20 nine noded small or large strain solid elements (A, B), 4564 fluid elements, 20 beam elements (C); (a) build-up of oscillations from the rest, (b) periodic long term responses.

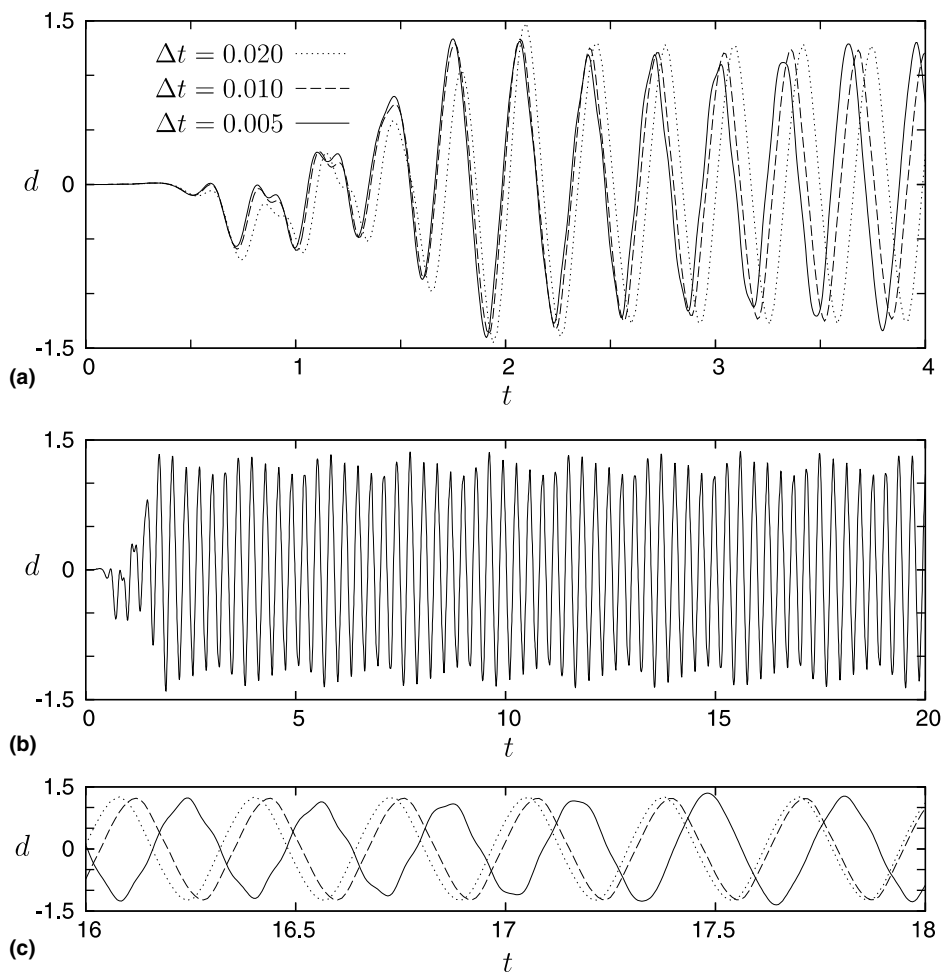


Fig. 8. Flow induced vibrations of a flexible beam: vertical displacement d of the tip of the structure; 4336 fluid elements, 20 nine noded small strain solid elements (A), different time step sizes Δt ; (a) build-up of oscillations from rest, (b) oscillations for small time step $\Delta t = 0.005$, (c) periodic long term responses.

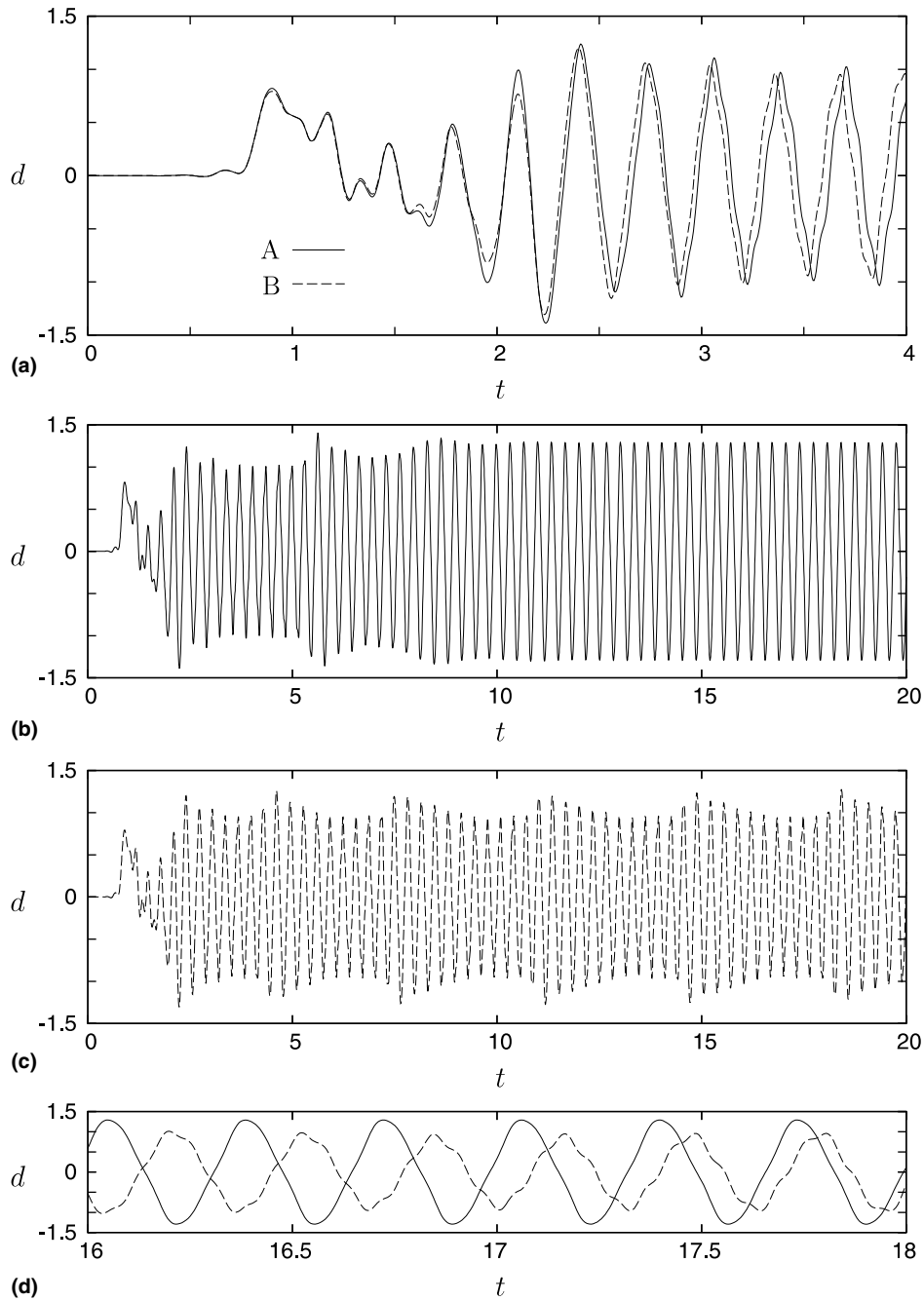


Fig. 9. Flow induced vibrations of a flexible beam: vertical displacement d of the tip of the structure; $\Delta t = 0.005$; 12,330 fluid elements, 20 nine noded small or large strain solid elements (A,B); (a) build-up of oscillations from rest, (b) oscillations for small strain model, (c) oscillations for large strain model, (d) periodic stable long term responses.

The fluid domain is discretised with 8658 elements. A detail of the mesh is given in Fig. 12. The mesh update in the ALE region is performed on the basis of the pseudo-elastic strategy discussed in Section 4.1 with $\mu^m = K^m = 1$. The membrane is modelled with 25 linear geometrically exact finite elements. The interface degrees of freedom coincide with those of the membrane. The time integration parameters are set to $\rho_\infty^f = \rho_\infty^s = 0.8$ for both the fluid and the membrane. First, the equilibrium configuration associated with $\bar{u}_{in} = 0$ is computed. This configuration depends only on the external pressure p_{ext} and the membrane stiffness. At time instant $t = 100$, the inflow velocity is then raised instantaneously from zero to $\bar{u}_{in} = 1$. For $100 < t < 150$, the time step size is set to $\Delta t = 0.1$, whereas for $t > 150$ different time step sizes are considered, in order to study the effect of Δt on the long term solution.

The diagrams in Fig. 13 show the evolution of the vertical displacement of point C of the membrane in time. Some vorticity plots are presented in Fig. 14. The convergence of the residuals for a typical time step is illustrated in Table 3.

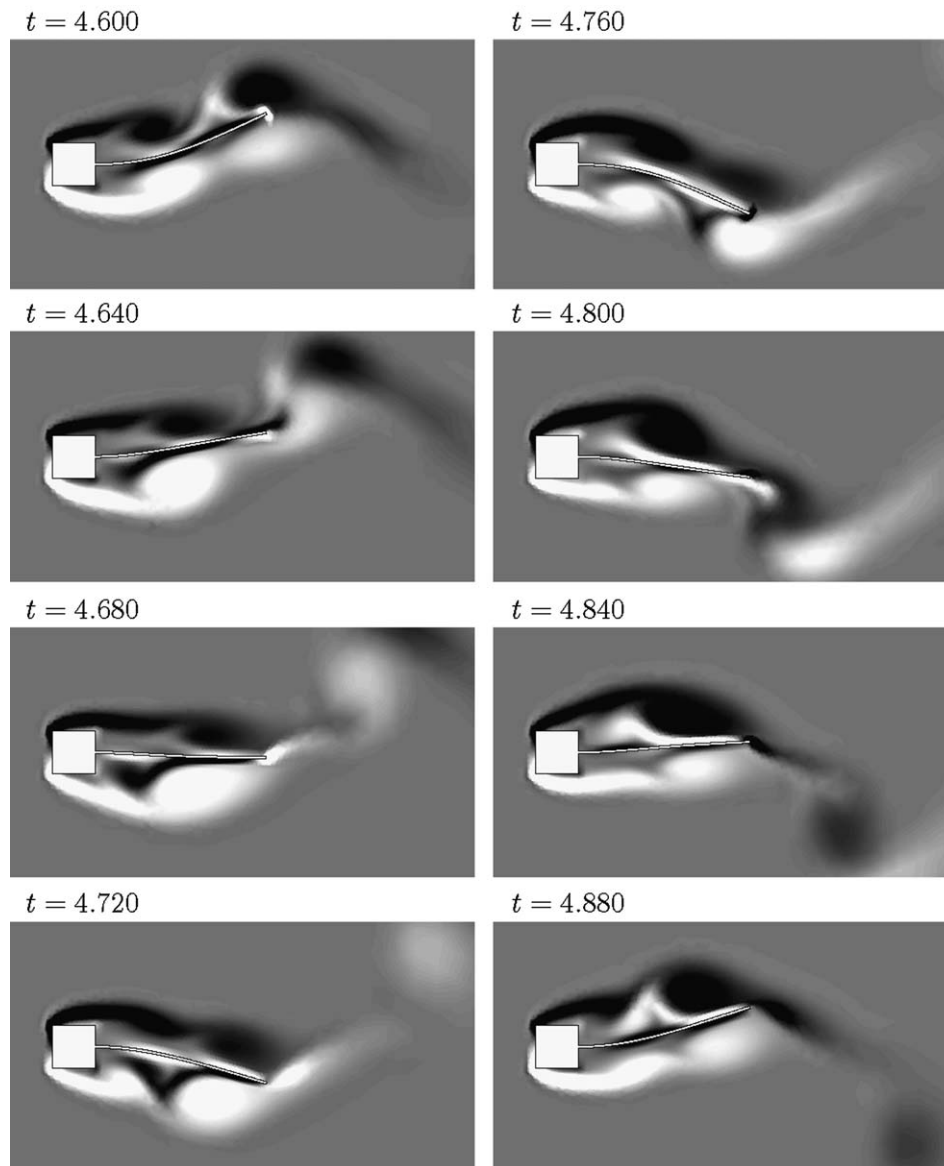


Fig. 10. Flow induced vibrations of a flexible beam: Typical vorticity distribution during stable long term oscillations, 4336 fluid finite elements, 20 small strain solid continuum elements (A), $\Delta t = 0.005$, $\text{vort}(u^h) \leq -150 \rightarrow \text{black}$, $\text{vort}(u^h) \geq +150 \rightarrow \text{white}$.

The following observations are made on the basis of the numerical results:

- The sudden increase of the inflow velocity from zero to \bar{u}_{in} causes the propagation of a pressure wave through the channel. The membrane acts like a buffer and temporarily forms a large bubble. The internal forces of the membrane and the external pressure soon reduce the extreme membrane displacements to more moderate values and, at about $t = 150$, the fluid flow and the deformation of the membrane seem to take an unsteady periodic long term response, which is characterised by the periodic necking of the downstream half of the membrane and the separation of vortices from the membrane surface, whenever the necking is maximal. This behaviour is illustrated in Figs. 13 and 14. A similar solution is obtained by Heil [57], who employs a different numerical model for the membrane.
- Fig. 13(b) shows that the long term responses obtained for the time step sizes $\Delta t = 0.02$ and $\Delta t = 0.50$ deviate only by a small amount.
- The convergence of the residuals is observed to be very good. Table 3 shows the residuals of a typical time instant obtained with the large time increment $\Delta t = 1.00$. Note that the table does not display any residuals of the solid solver. This is due to the fact, that all degrees of freedom of the membrane are, in fact, degrees of freedom of the interface. Thus, step 3 in Box 1 does not apply, and some expressions in the formula of step 5 vanish. The partitioned Newton–Raphson procedure may be considered to reduce to a monolithic scheme in this special case.

Table 1

Flow induced vibrations of a flexible beam: periodic long term response, typical convergence of the absolute residuals, 4564 fluid elements, 20 geometrically exact beam elements (C), $\Delta t = 0.005$, $t = 19.780$

I	II	III	IV							
2		1.00	No conv.							
		0.50	No conv.							
		0.25	3.6E+2	1.4E+2	3.7E+1	4.4E+0	1.2E-1	1.0E-4	9.0E-11	
		0.50	3.9E+2	1.5E+2	4.5E+1	5.0E+0	1.4E-1	1.2E-4	1.1E-10	
		0.75	4.3E+2	1.7E+2	5.6E+1	7.7E+0	5.0E-1	2.4E-3	5.1E-8	
		1.00	4.8E+2	1.9E+2	9.8E+1	2.7E+1	3.2E+0	8.5E-2	7.0E-5	7.1E-11
3			9.1E-1	1.8E-9						
4	7.4E+1									
2		1.00	6.9E+0	2.8E-1	5.1E-4	2.0E-9				
3			2.3E+1	2.5E-5	5.6E-13					
4	1.1E+0									
2		1.00	1.9E-1	2.9E-4	5.9E-10					
3			7.9E-1	2.4E-9						
4	1.2E-2									
2		1.00	1.3E-4	1.1E-10						
3			3.2E-4	5.8E-13						
4	2.9E-7									

Column I: identifies step in Box 1, fluid mesh solver (2), solid solver (3), residual of combined fluid + interface solver (4).

Column II: combined fluid + interface residual.

Column III: increment cutting in the fluid mesh solver.

Column IV: residuals of fluid mesh solver and solid solver.

Table 2

Flow induced vibrations of a flexible beam: periodic long term response, typical convergence of the absolute residuals, 12,330 fluid elements, 20 large strain solid continuum elements (B), $\Delta t = 0.005$, $t = 19.985$

I	II	III	IV						
2		1.0000	No conv.						
		0.5000	No conv.						
		0.2500	No conv.						
		0.1250	No conv.						
		0.0625	6.2E+2	2.6E+2	4.6E+1	2.4E+0	9.4E-3	1.7E-7	6.8E-10
		0.1250	6.2E+2	2.6E+2	4.6E+1	2.4E+0	9.4E-3	1.6E-7	6.8E-10
		0.1875	6.2E+2	2.6E+2	4.6E+1	2.4E+0	9.3E-3	1.6E-7	6.6E-10
							
							
		0.6875	6.4E+2	2.6E+2	4.6E+1	2.4E+0	8.8E-3	1.3E-7	6.8E-10
		0.7500	6.4E+2	2.6E+2	4.6E+1	2.4E+0	8.8E-3	1.3E-7	6.7E-10
		0.8125	6.4E+2	2.6E+2	4.6E+1	2.4E+0	8.8E-3	1.3E-7	6.7E-10
		0.8750	6.4E+2	2.6E+2	4.6E+1	2.4E+0	8.8E-3	1.3E-7	6.5E-10
		0.9375	6.4E+2	2.6E+2	4.6E+1	2.4E+0	8.8E-3	1.3E-7	6.6E-10
		1.0000	6.4E+2	2.6E+2	4.6E+1	2.4E+0	8.8E-3	1.2E-7	6.8E-10
3			1.3E+2	1.0E-5	3.4E-9				
4	5.9E+3								
2		1.00	No conv.						
		0.50	2.1E+2	8.5E+1	1.1E+1	2.4E-1	1.2E-4	6.4E-10	
		1.00	2.1E+2	8.5E+1	1.1E+1	2.3E-1	1.1E-4	6.3E-10	
3			9.3E+4	1.8E+2	2.7E-3	2.0E-9			
4	1.7E+1								
2		1.00	5.4E+1	2.3E+0	6.3E-3	6.1E-08			
3			2.7E+4	7.4E+1	2.2E-3	1.6E-09			
4	1.6E-1								
2		1.00	5.6E-1	2.8E-4	6.5E-10				
3			2.0E+2	6.6E-3	3.0E-9				
4	4.6E-5								

Column I: identifies step in Box 1, fluid mesh solver (2), solid solver (3), residual of combined fluid + interface solver (4).

Column II: combined fluid + interface residual.

Column III: increment cutting in the fluid mesh solver.

Column IV: residuals of fluid mesh solver and solid solver.

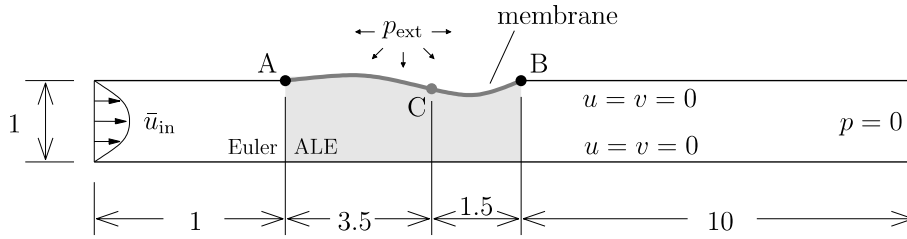


Fig. 11. Flow through a channel with a flexible wall: geometry of the problem and boundary conditions.

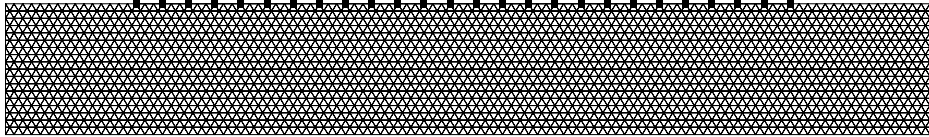


Fig. 12. Flow through a channel with a flexible wall: detail of fluid mesh with 8658 and membrane mesh with 25 finite elements.

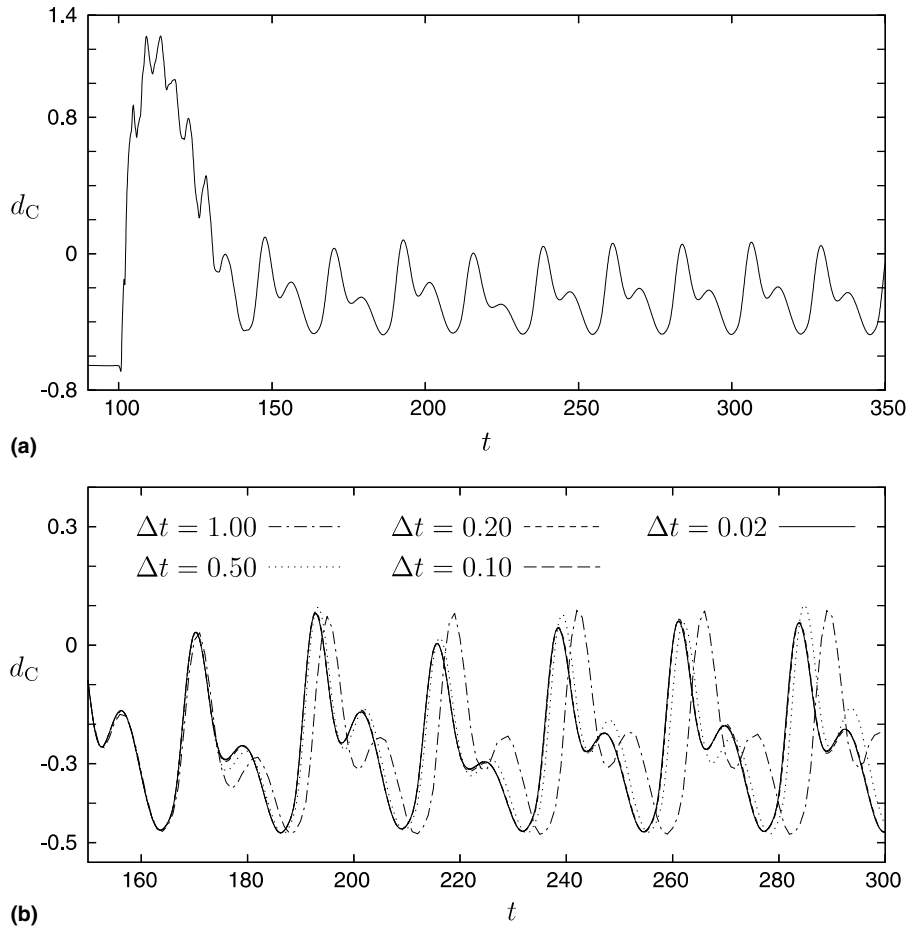


Fig. 13. Flow through a channel with a flexible wall: evolution of vertical displacement d_C of point C of the membrane in time; transition from initial disturbances to stable long term behaviour for $\Delta t = 0.10$ (a), long term response for different time step sizes (b).

9.3. Flow through a flexible pipe

This example is concerned with the flow through a flexible circular pipe. The physics of this class of problems, which is extremely relevant in the area of biomechanics, is very complex and very sensitive to the problem boundary conditions and

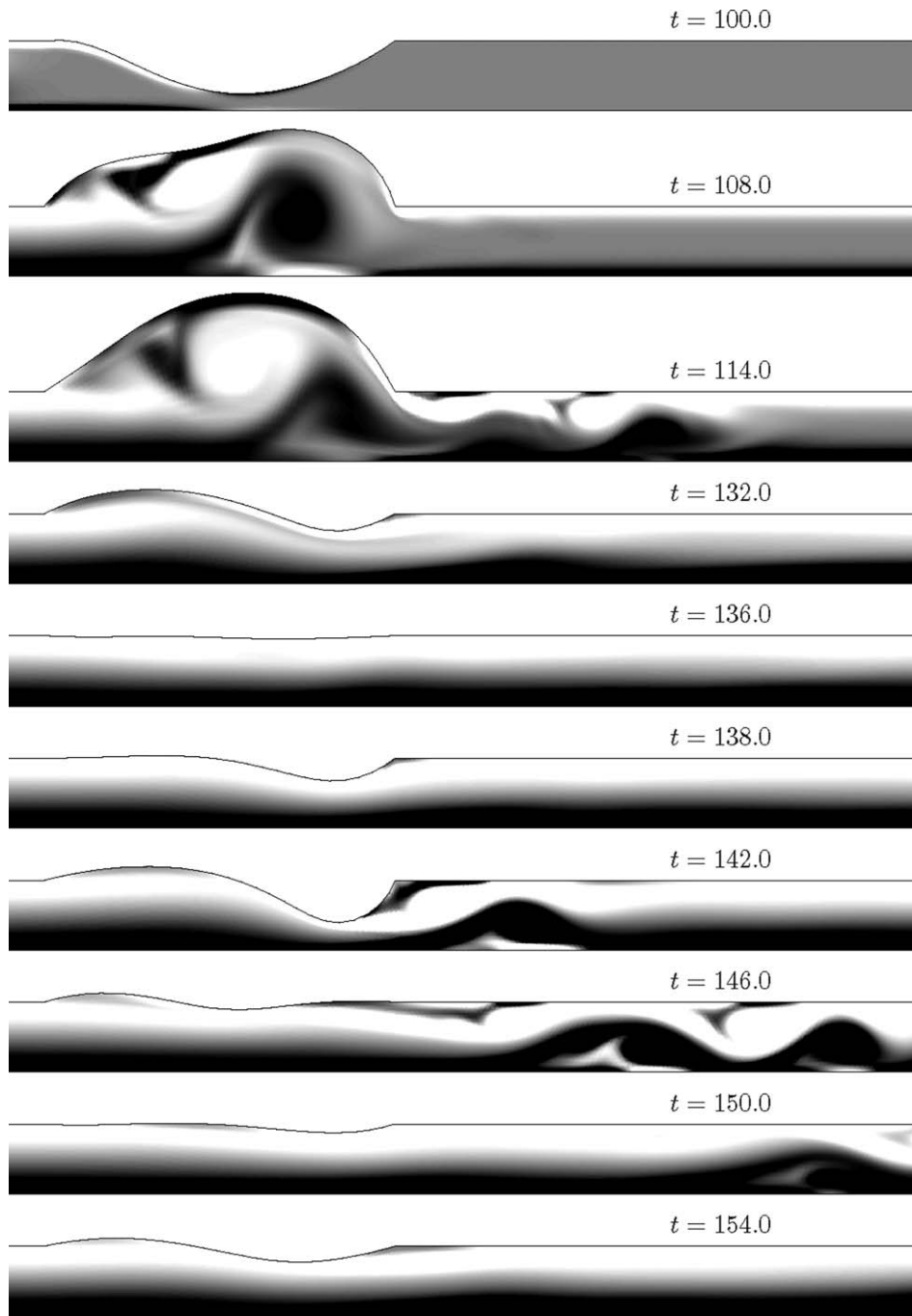


Fig. 14. Flow through a channel with a flexible wall: vorticity distribution at different time instants; $\Delta t = 0.01$, $\text{vort}(\mathbf{u}^h) \leq -3 \rightarrow \text{black}$, $\text{vort}(\mathbf{u}^h) \geq +3 \rightarrow \text{white}$.

the material properties of the pipe. Thus, for the sake of brevity, we restrict this subsection to a preliminary study of the problem with focus on the efficiency of the methodology developed in this work.

The pipe consists of Neo–Hookean elastic material described by (60). At the inflow end, the orifice is fixed in space, whereas the outflow end is free to expand or contract, but fixed in the direction of the pipe axis. The inflow velocity profile corresponds to undisturbed Poiseuille flow with the maximum velocity $u_{\max}(t)$. The geometry and the boundary conditions of the problem are displayed in Fig. 15. Axisymmetric conditions are assumed in this study.

The viscosity and the density of the fluid are $\mu^f = 0.0101 \text{ g (cm s)}^{-1}$ and $\rho^f = 0.998 \text{ g cm}^{-3}$, whereas the material parameters of the pipe are chosen as $\mu^s = 0.1 \text{ N mm}^{-2}$, $K^s = 5 \text{ N mm}^{-2}$ and $\rho^s = 0.1 \text{ g cm}^{-3}$. The inflow velocity varies in time according to

$$u_{\max}(t) = \bar{u}(1 - \cos(\omega t)), \tag{62}$$

Table 3

Flow through a channel with a flexible wall: convergence of the absolute residuals of a typical large time step, $\Delta t = 1.0$, $t = 340$; note that the solid solver does not need to be evoked since all degrees of freedom of the membrane are interface degrees of freedom

I	II	III	IV							
2		1.000	No conv.							
		0.500	No conv.							
		0.250	1.6E+0	6.9E-1	2.6E-1	6.3E-2	5.3E-3	4.2E-5	2.7E-9	
		0.500	3.0E+0	1.4E+0	6.3E-1	2.7E-1	8.3E-2	1.1E-2	1.8E-4	5.5E-8
		0.625	4.7E-1	1.1E-1	1.1E-2	1.4E-4	2.9E-8			
		0.750	5.0E-1	1.2E-1	1.4E-2	2.4E-4	9.2E-8			
		0.875	5.3E-1	1.4E-1	1.8E-2	4.3E-4	3.1E-7	1.8E-13		
		1.000	5.7E-1	1.6E-1	2.3E-2	7.8E-4	1.1E-6	2.1E-12		
4	2.4E+0									
2		1.0	1.5E+0	6.0E-1	2.3E-1	5.1E-2	2.8E-3	8.9E-6	8.6E-11	
4	4.9E-1									
2		1.0	4.3E-1	1.0E-1	7.7E-3	6.5E-5	5.4E-9			
4	4.7E-2									
2		1.0	1.1E-2	4.2E-5	1.9E-9					
4	2.7E-4									
2		1.0	3.7E-5	6.8E-10						
4	4.5E-9									

Column I: identifies step in Box 1, fluid mesh solver (2), residual of combined fluid + interface solver (4).

Column II: combined fluid + interface residual.

Column III: increment cutting in the fluid mesh solver.

Column IV: residuals of fluid mesh solver.

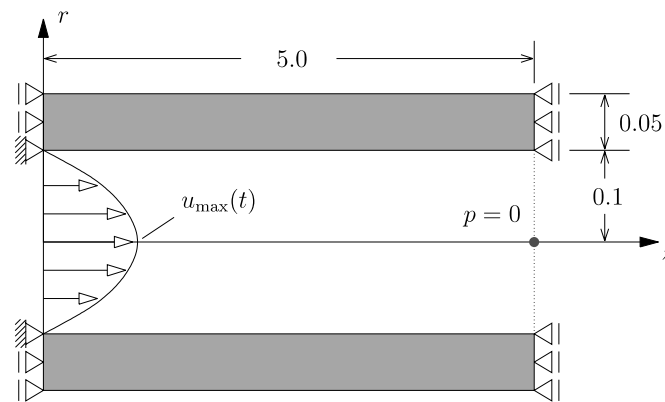


Fig. 15. Flow through a flexible pipe: geometry and boundary conditions.

which corresponds to a sequence of sinusoidal impulses. We choose $\bar{u} = 5 \text{ cm s}^{-1}$ and $\omega = 10 \text{ s}^{-1}$. The choice of the parameters is arbitrary and serves only the demonstrational purpose of this numerical study.

The fluid domain is modelled with 3250 axisymmetric finite elements. The pipe wall is represented by 450 eight noded axisymmetric quadrilateral elements, each of which is integrated with four Gauß points. A detail of the spatial discretisation is shown in Fig. 16, in which the independent interface nodes are highlighted. The ALE region is identical with the entire fluid domain and the mesh update is based on the quality criteria (19). The time integration parameters are set to $\rho_{\infty}^f = 0.85$ and $\rho_{\infty}^s = 0.7$. The simulations are performed for $\Delta t = 0.02 \text{ s}$.

The diagram in Fig. 17 shows the evolution in time of the prescribed rate of inflow and the resulting rate of outflow of fluid volume. Several typical mesh configurations of the pipe are displayed in Fig. 18.

We make the following observations:

- After approximately 10 inflow cycles the outflow shows a stable long term response, which is characterized by the equality of the average inflow and outflow rates. Clearly, the deformation of the flexible pipe damps out the variations of the inflow.
- The convergence of the residuals is observed to be asymptotically quadratic.

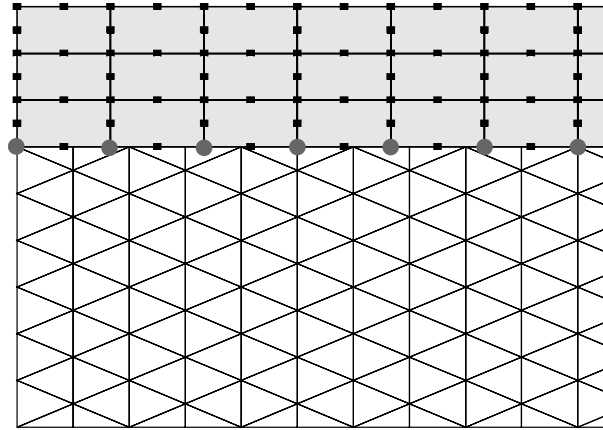


Fig. 16. Flow through a flexible pipe: detail of fluid and solid meshes, interface nodes are highlighted.

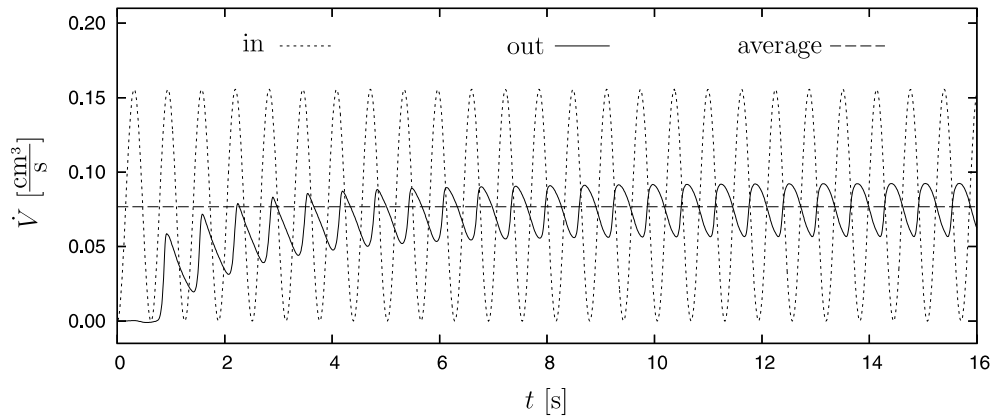


Fig. 17. Flow through a flexible pipe: evolution of flow rates in time.

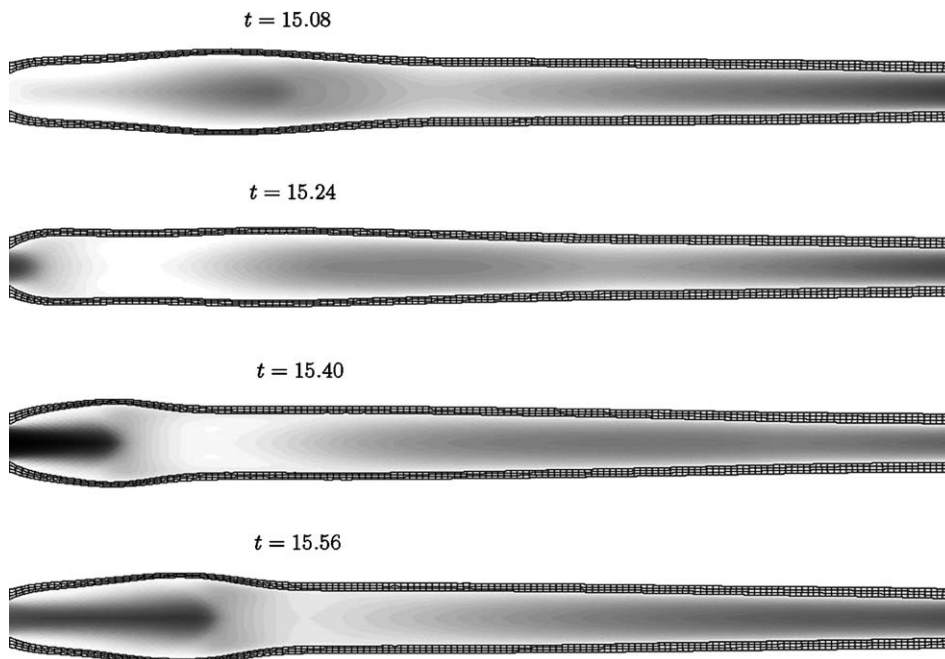


Fig. 18. Flow through a flexible pipe: typical configurations of the pipe and distribution of axial fluid velocity, $u_z \leq 0 \text{ cm s}^{-1} \rightarrow \text{white}$, $u_z \geq 10 \text{ cm s}^{-1} \rightarrow \text{black}$.

10. Conclusions

A computational fully implicit strategy for fluid–structure interaction has been presented. Numerical examples have been provided, which give evidence of its robustness and efficiency. The discretisation of time and space can, to a wide extent, be refined independently.

The adopted computational framework allows the independent discretisation of fluid, solid and interface. The solution strategy of the coupled system, which relies on the separation of the mesh solver, the structural solver and the combined fluid + interface solver, is based on consistent linearisation, and renders asymptotically quadratic convergence of the residuals. However, we note that the methodology presented requires careful and tedious computer implementation.

The strategy seems well suited for the modelling of the interaction of fluid flow with very flexible structures, which undergo large displacements.

It should be mentioned that, although applications presented in this work have been restricted to two-dimensional configurations, no conceptual difficulties exist in employing the described strategy in three-dimensional situations.

For a moderate number of interface degrees of freedom n^i , the overall requirements on computational time and computer memory seem very competitive. The efficiency of the developed methodology for problems with larger n^i needs further investigation. The detailed report assessing the efficiency of the developed computational framework for fluid–structure interaction is planned for future publications.

Acknowledgment

This work is partially founded by EPSRC of UK under Grant No. GR/R92318/01. This support is gratefully acknowledged.

References

- [1] R.D. Blevins, *Flow-Induced Vibration*, second ed., Krieger, Malabar, FL, 2001.
- [2] R. Ohayon, C. Felippa (Eds.), *Advances in Computational Methods for Fluid–Structure Interaction and Coupled Problems*, *Comput. Methods Appl. Mech. Engrg.* 190 (1998) 2977–3292.
- [3] W. Dettmer, D. Perić, A computational framework for free surface flows accounting for surface tension, *Comput. Methods Appl. Mech. Engrg.*, in press, doi:10.1016/j.cma.2004.07.057.
- [4] W. Dettmer, D. Perić, A computational framework for fluid–rigid body interaction: finite element formulation and applications, *Comput. Methods Appl. Mech. Engrg.* 195 (2006) 1633–1666.
- [5] W. Dettmer, *Finite element modelling of fluid flow with moving free surfaces and interfaces including fluid–solid interaction*, Ph.D. thesis, University of Wales Swansea, 2004.
- [6] A.N. Brooks, T.J.R. Hughes, Streamline-upwind/Petrov–Galerkin formulations for convection dominated flows with particular emphasis on the incompressible Navier–Stokes equations, *Comput. Methods Appl. Mech. Engrg.* 32 (1982) 199–259.
- [7] T.J.R. Hughes, L.P. Franca, G.M. Hulbert, A new finite element formulation for computational fluid dynamics: VIII. The Galerkin/least-squares method for advective–diffusive equations, *Comput. Methods Appl. Mech. Engrg.* 73 (1989) 173–189.
- [8] T.J.R. Hughes, L.P. Franca, M. Balestra, A new finite element formulation for computational fluid dynamics: V. Circumventing the Babuska–Brezzi condition: a stable Petrov–Galerkin formulation of the Stokes problem accommodating equal-order interpolations, *Comput. Methods Appl. Mech. Engrg.* 59 (1986) 85–99.
- [9] T.E. Tezduyar, S. Mittal, S.E. Ray, R. Shih, Incompressible flow computations with stabilized bilinear and linear equal-order-interpolation velocity–pressure elements, *Comput. Methods Appl. Mech. Engrg.* 95 (1992) 221–242.
- [10] J.-J. Droux, T.J.R. Hughes, A boundary integral modification of the Galerkin/least-squares formulation for the Stokes problem, *Comput. Methods Appl. Mech. Engrg.* 113 (1994) 173–182.
- [11] K.E. Jansen, S.S. Collis, F. Shakib, A better consistency for low-order stabilized finite element methods, *Comput. Methods Appl. Mech. Engrg.* 174 (1999) 153–170.
- [12] T.E. Tezduyar, Y. Osawa, Finite element stabilization parameters computed from element matrices and vectors, *Comput. Methods Appl. Mech. Engrg.* 190 (2000) 411–430.
- [13] A. Masud, T.J.R. Hughes, A space–time Galerkin/least-squares finite element formulation of the Navier–Stokes equations for moving domain problems, *Comput. Methods Appl. Mech. Engrg.* 146 (1997) 91–126.
- [14] P. Hansbo, A Crank–Nicolson type space–time finite element method for computing on moving meshes, *J. Comput. Phys.* 159 (2000) 274–289.
- [15] M. Behr, T.E. Tezduyar, The shear slip mesh update method, *Comput. Methods Appl. Mech. Engrg.* 174 (1999) 261–274.
- [16] V. Kalro, T.E. Tezduyar, A parallel 3D computational method for fluid–structure interactions in parachute systems, *Comput. Methods Appl. Mech. Engrg.* 190 (2000) 321–332.
- [17] D. Perić, S. Slijepčević, Computational modelling of viscoplastic fluids based on a stabilised finite element method, *Engrg. Comput.* 18 (2001) 577–591.
- [18] W. Dettmer, P.H. Saksono, D. Perić, On a finite element formulation for incompressible Newtonian fluid flows on moving domains in the presence of surface tension, *Commun. Numer. Methods Engrg.* 19 (2003) 659–668.
- [19] W. Wall, *Fluid–Struktur-Interaktion mit Stabilisierten Finiten Elementen*, Ph.D. thesis, Universität Stuttgart, 1999.
- [20] L.P. Franca (Ed.), *Advances in Stabilised Methods in Computational Mechanics*, *Comput. Methods Appl. Mech. Engrg.* 166 (1998) 1–182.
- [21] H.G. Matthies, Partitioned analysis of coupled systems, in: *5th International Conference on Computation of Shell and Spatial Structures*, Salzburg, Austria, 2005.

- [22] C.W. Hirt, A.A. Amsden, J.L. Cook, An arbitrary Lagrangian–Eulerian computing method for all flow speeds, *J. Comput. Phys.* 14 (1974) 227–253.
- [23] T.J.R. Hughes, W.K. Liu, T.K. Zimmermann, Lagrangian–Eulerian finite element formulation for incompressible viscous flows, *Comput. Methods Appl. Mech. Engrg.* 29 (1981) 329–349.
- [24] J. Donea, Arbitrary Lagrangian–Eulerian finite element methods, in: T. Belytschko, T.J.R. Hughes (Eds.), *Computational Methods for Transient Analysis*, Elsevier, Amsterdam, 1983, pp. 473–516.
- [25] B. Ramaswamy, M. Kawahara, Arbitrary Lagrangian–Eulerian finite element method for unsteady, convective, incompressible viscous free surface fluid flow, *Int. J. Numer. Methods Fluids* 7 (1987) 1053–1075.
- [26] B. Ramaswamy, Numerical simulation of unsteady viscous free surface flow, *J. Comput. Phys.* 90 (1990) 396–430.
- [27] A. Huerta, W.K. Liu, Viscous flow with large free surface motion, *Comput. Methods Appl. Mech. Engrg.* 69 (1988) 277–324.
- [28] A. Soulaïmani, M. Fortin, G. Dhaut, Y. Ouellet, Finite element simulation of two- and three-dimensional free surface flows, *Comput. Methods Appl. Mech. Engrg.* 86 (1991) 265–296.
- [29] P.A. Sackinger, P.R. Schunk, R.R. Rao, A Newton–Raphson pseudo-solid domain mapping technique for free and moving boundary problems: a finite element implementation, *J. Comput. Phys.* 125 (1996) 83–103.
- [30] A. Soulaïmani, Y. Saad, An arbitrary Lagrangian–Eulerian finite element method for solving three-dimensional free surface flows, *Comput. Methods Appl. Mech. Engrg.* 162 (1998) 79–106.
- [31] H. Braess, P. Wriggers, Arbitrary Lagrangian Eulerian finite element analysis of free surface flow, *Comput. Methods Appl. Mech. Engrg.* 190 (2000) 95–109.
- [32] T. Belytschko, W.K. Liu, B. Moran, *Nonlinear Finite Elements for Continua and Structures*, John Wiley & Sons, Chichester, UK, 2000.
- [33] T.E. Tezduyar, M. Behr, J. Liou, A new strategy for finite element computations involving moving boundaries and interfaces—The deforming-spatial-domain/space–time-procedure: I. The concept and the preliminary numerical tests, *Comput. Methods Appl. Mech. Engrg.* 94 (1992) 339–351.
- [34] T.E. Tezduyar, M. Behr, S. Mittal, J. Liou, A new strategy for finite element computations involving moving boundaries and interfaces—The deforming-spatial-domain/space–time-procedure: II. Computation of free-surface flows, two-liquid flows, and flows with drifting cylinders, *Comput. Methods Appl. Mech. Engrg.* 94 (1992) 353–371.
- [35] J. Chung, G.M. Hulbert, A time integration algorithm for structural dynamics with improved numerical dissipation: the generalized- α method, *J. Appl. Mech.* 60 (1993) 371–375.
- [36] K.E. Jansen, C.H. Whiting, G.M. Hulbert, A generalized α -method for integrating the filtered Navier–Stokes equations with a stabilized finite element method, *Comput. Methods Appl. Mech. Engrg.* 190 (2000) 305–319.
- [37] W. Dettmer, D. Perić, An analysis of the time integration algorithms for the finite element solutions of incompressible Navier–Stokes equations based on a stabilised formulation, *Comput. Methods Appl. Mech. Engrg.* 192 (2003) 1177–1226.
- [38] C.A. Felippa, K.C. Park, C. Farhat, Partitioned analysis of coupled mechanical systems, *Comput. Methods Appl. Mech. Engrg.* 190 (2001) 3247–3270.
- [39] H.G. Matthies, R. Niekamp, J. Steindorf, *Algorithms for Strong Coupling Procedures*, preprint, 2004.
- [40] H.G. Matthies, J. Steindorf, *Strong Coupling Methods*, Technical University Brunswick, Institute of Scientific Computing, 2002, Informatikbericht 2002–06.
- [41] T.E. Tezduyar, *Methods for computation of moving boundaries and interfaces*, ECCOMAS 2004, Jyväskylä, Finland, 2004.
- [42] T.E. Tezduyar, S. Sathe, R. Keedy, K. Stein, *Space–time techniques for finite element computation of flows with moving boundaries and interfaces*, in: III International Congress on Numerical Methods in Engineering and Applied Sciences, Monterrey, Mexico, 2004.
- [43] E. Onate, A stabilized finite element method for incompressible viscous flows using a finite increment calculus formulation, *Comput. Methods Appl. Mech. Engrg.* 182 (2000) 355–370.
- [44] T.E. Tezduyar, M. Behr, S. Mittal, A.A. Johnson, *Computation of unsteady incompressible flows with the stabilized finite element methods—space–time formulations, iterative strategies and massively parallel implementations*, *New Methods in Transient Analysis*, PVP-Vol. 246/AMD-Vol. 143, ASME, New York, 1992, pp. 7–24.
- [45] P.Z. Bar-Yoseph, S. Mereu, S. Chippada, V.J. Kalro, Automatic monitoring of element shape quality in 2-D and 3-D computational mesh dynamics, *Comput. Mech.* 27 (2001) 378–395.
- [46] C. Degand, C. Farhat, A three-dimensional torsional spring analogy method for unstructured dynamic meshes, *Comput. Struct.* 80 (2002) 305–316.
- [47] C. Farhat, M. Lesoinne, P. Le Tallec, Load and motion transfer algorithms for fluid/structure interaction problems with non-matching discrete interfaces: momentum and energy conservation, optimal discretisation and application to aeroelasticity, *Comput. Methods Appl. Mech. Engrg.* 157 (1998) 95–114.
- [48] C. Bernardi, Y. Maday, A.T. Patera, A new non-conforming approach to domain decomposition: the mortar finite element method, in: H. Brezis, J.L. Lions (Eds.), *Nonlinear Partial Differential Equations and their Applications*, Pitman and Wiley, 1992, pp. 13–51.
- [49] P. Hansbo, J. Hermansson, Nitsche’s method for coupling non-matching meshes in fluid–structure vibration problems, *Comput. Mech.* 32 (2003) 134–139.
- [50] P. Hansbo, J. Hermansson, T. Svedberg, Nitsche’s method combined with space–time finite elements for ALE fluid–structure interaction problems, *Comput. Methods Appl. Mech. Engrg.* 193 (2004) 4195–4206.
- [51] W.A. Wall, E. Ramm, Fluid–structure interaction based upon a stabilized (ALE) finite element method, in: S.R. Idelsohn, E. Onate (Eds.), *4th World Congress on Computational Mechanics*, CIMNE, Barcelona, Spain, *Computational mechanics—New trends and applications*, Buenos Aires, Argentina, 1998.
- [52] B. Hübner, E. Walhorn, D. Dinkler, *Strongly Coupled Analysis of Fluid–Structure Interaction Using Space–Time Finite Elements*, ECCM 2001, Cracow, Poland.
- [53] B. Hübner, E. Walhorn, D. Dinkler, A monolithic approach to fluid–structure interaction using space–time finite elements, *Comput. Methods Appl. Mech. Engrg.* 193 (2004) 2087–2104.
- [54] J. Steindorf, *Partitionierte Verfahren für Probleme der Fluid–Struktur Wechselwirkung*, Ph.D. thesis, Technische Universität Braunschweig, Mechanik-Zentrum, 2003.
- [55] O.C. Zienkiewicz, R.L. Taylor, *The Finite Element Method*, fifth ed., Butterworth-Heinemann, Oxford, UK, 2000.
- [56] X.Y. Luo, T.J. Pedley, A numerical simulation of unsteady flow in a two-dimensional collapsible channel, *J. Fluid Mech.* 314 (1996) 191–225.
- [57] M. Heil, An efficient solver for the fully coupled solution of large-displacement fluid–structure interaction problems, *Comput. Methods Appl. Mech. Engrg.* 193 (2004) 1–23.